Northern North Atlantic climate variability controls on ocean carbon sinks in EC-Earth3-CC

Anna Pedersen[1,2], Carolin R. Löscher[1], Steffen M. Olsen[2]

[1]Nordcee, University of Southern Denmark, Odense, 5230, Denmark
[2]Danish Meteorological Institute, National Centre for Climate Research, Copenhagen, 2100, Denmark

Correspondence to: Anna Pedersen (annapedersen@biology.sdu.dk)

Abstract

The northern North Atlantic is an important net sink of atmospheric CO_2, though atmosphere–ocean CO_2 fluxes exhibit substantial variability across different timescales. The underlying drivers of this variability remain poorly understood across both temporal and regional scales. Here, we investigate interannual to decadal CO_2 flux variability in the northern North Atlantic using historical simulations from the EC-Earth3-CC model. We assess the role of key dynamical and physical processes in shaping CO_2 flux variability across five regions: the Nordic Seas, eastern Nordic Seas, the eastern and western subpolar North Atlantic, and the full North Atlantic. Our analysis reveals that physical parameters—including sea ice concentration (SIC), sea surface temperature (SST), sea surface salinity (SSS), and wind stress—along with dynamical processes related to ocean mixing and circulation, play a central role in regulating CO_2 flux variability. Using regression analysis, we demonstrate that these drivers exert regionally and temporally varying influences, with our models achieving high R^2 values indicating a strong degree of explanation for CO_2 flux variability. The regression models capture interannual variability more effectively than decadal variability, highlighting the dominant role of short-term fluctuations in shaping CO_2 flux dynamics. Overall, our results demonstrate that the predictors of CO_2 flux variability are both spatially and temporally dependent. We find that CO_2 flux variability cannot be fully explained by simple linear correlations with individual predictors but instead arises from complex interactions among multiple physical and dynamical processes. Notably, CO_2 flux variability is particularly sensitive to changes in certain predictors, such as wind stress, consistent with expectations based on the gas transfer equation used to compute atmosphere–ocean CO_2 fluxes.

Deleted: ir

Deleted: -sea

Deleted: ir-sea

1. Introduction

30 The northern North Atlantic is a net sink of atmospheric carbon dioxide (CO_2; Fig. 1a; Gruber et al., 2002; Takahashi et al., 2009, Yu et al., 2019). This sink is primarily driven by the combined effects of the solubility pump and the biological carbon pump. The solubility pump enhances CO_2 uptake through two key mechanisms: (1) the cooling of northward-flowing warm waters, which increases CO_2 solubility at the surface, and (2) the formation of dense, cold deep water at high latitudes, which transports CO_2-enriched surface waters into the ocean interior as part of the Atlantic thermohaline circulation (Volk et al.,

35 1985). The biological carbon pump further contributes by fixating carbon through photosynthesis and primary production (PP), exporting organic carbon to the deep ocean, and maintaining a net sink of atmospheric CO_2 in the region (Sigman and Boyle, 2000; Boyd and Trull, 2007; Sanders et al., 2014). Currently, the North Atlantic absorbs a significant fraction of anthropogenic CO_2 emissions, accounting for approximately one-quarter to one-third of global anthropogenic carbon uptake (Khatiwala et al., 2009; Sabine et al., 2004; Breeden and McKinley, 2016; Le Quéré et al., 2018; Gruber et al., 2019). In

40 contrast, the global ocean uptake is around 25% of annual emissions due to outgassing in some ocean regions (Fig. 1; Landschützer et al., 2016; Mikaloff Fletcher et al., 2006; Khatiwala et al., 2013; Le Quéré et al., 2015; Friedlingstein et al., 2023; Gruber et al., 2023; Terhaar et al., 2022).

Beyond these large-scale mechanisms, the strength of the North Atlantic CO_2 sink varies seasonally and interannually, influenced by ocean-atmosphere interactions. Biological productivity peaks in spring and summer, enhancing

45 CO_2 drawdown, while wintertime cooling promotes solubility-driven uptake (Ardyna and Arrigo 2020). These processes are modulated by climate variability, particularly the North Atlantic Oscillation (NAO) and the Atlantic Multidecadal Oscillation (AMO; Leseurre et al., 2020). Additionally, physical processes such as warming and cooling cycles, deep convection, and changes in ocean circulation and water masses in the subpolar gyre (SPG) play a crucial role in regulating air-sea CO_2 fluxes. These physical drivers are closely linked to NAO and AMO variability, further influencing regional CO_2

50 uptake dynamics (Chafik et al., 2019; Desbruyères et al., 2015). Breeden and McKinley (2016) show that a North Atlantic basin-average sea surface temperature (SST) is associated with the leading mode of surface ocean pCO_2 variability based on an analysis of a regional model. The SST signal is affected by an upward trend due to greenhouse gas emissions and a signal of internal variability due to the AMO (Kerr, 2000). Furthermore, they establish that physical (in contrast to the chemical) variability is the dominant driver of variability in the North Atlantic surface ocean carbon cycle. During a positive phase of

55 the AMO an increase in sea (surface) temperature increases pCO_2 due to the reduction in solubility (an increase in the fugacity of CO_2, fCO_2) resulting in a reduced flux of CO_2 into the ocean (also seen in Breeden and McKinley (2016)). Studies show that on a decadal scale the AMO and fCO_2 variability in the SPG correlates (Breeden and McKinley, 2016; Landschutzer et al., 2019; Leseurre et al., 2020): as the AMO enters a positive (warm) phase, reduced mixing (a shallowing of the mixed layer depth) results in a reduced supply of dissolved inorganic carbon (DIC) from the subsurface layers, a

60 process that dominates the effect of warming on the solubility and fCO_2. The surface ocean's ability to absorb anthropogenic carbon is primarily regulated by carbonate chemistry, particularly alkalinity (Broecker et al., 1979; Terhaar et al., 2022).

While increasing anthropogenic carbon generally enhances ocean carbon uptake, this relationship is moderated by rising global temperatures, which reduce solubility, and further influenced by decadal variability and long-term trends. However, the underlying drivers of these trends remain poorly understood (Terhaar, 2024).

65   The subpolar North Atlantic has experienced significant interannual to decadal variability in ventilation depth during the industrial period (Polyakov 2005; Holliday et al., 2020; Zou et al., 2023, Thomas and Zhang 2022). Recent studies highlight pronounced ocean variability in the Subpolar Gyre region, including the formation of cold and fresh anomalies. Holliday et al. (2020) documented a substantial freshening event in the eastern subpolar North Atlantic, the most significant in 120 years, attributed to wind-driven circulation changes that redistributed freshwater within the region.

70 Similarly, Zou et al. (2023) identified two sources of deep ocean variability in the central Labrador Sea, furthering our understanding of long-term property anomalies in the western subpolar North Atlantic. These findings underscore the SPG's dynamic nature and its sensitivity to both atmospheric and oceanic forcing. The SPG, a counterclockwise gyre system, plays a crucial role in modulating ocean circulation by introducing saline Atlantic Water into the northern North Atlantic. The North Atlantic Current follows the southern and eastern boundaries of the SPG, transporting warm, saline water from the

75 Gulf Stream into the northern North Atlantic and eventually the Arctic (Holliday et al., 2020; Daniault et al., 2016; Hátún et al., 2017). At the same time, freshwater from the Arctic is supplied to the SPG, contributing to temporal variability in ocean properties. These processes are key regulators of the AMOC (Holliday et al., 2020; Hátún et al., 2005, 2017). The strength of the SPG circulation strongly influences both physical and biological processes in the northern North Atlantic. A weak (strong) SPG leads to a shallowing (deepening) of sea surface height (SSH) and, consequently, a shallowing (deepening) of

80 the mixed layer depth (MLD). Additionally, a weak SPG contracts westward, allowing nutrient-poor subtropical waters to penetrate northward, warming the gyre and reducing primary production. In contrast, a strong SPG expands eastward, accumulates Arctic fresh and nutrient-rich water within the gyre system, increasing PP and solubility, and limits the intrusion of warm, saline Atlantic Water into the region (Häkkinen et al., 2013; Hátún et al., 2005, 2017; Foukal et al., 2017). Importantly, variations in SSS serve as an indicator of these gyre dynamics and ocean mixing processes, making it a valuable

85 indirect predictor of CO_2 flux variability. Changes in salinity reflect shifts in water mass distribution, stratification, and ventilation, all of which influence air-sea gas exchange. Therefore, monitoring SSS variability can provide critical insights into the mechanisms driving CO_2 flux variability in the North Atlantic (Thomas and Zhang, 2022).

      Understanding the vulnerability of the ocean carbon sink to future climatic changes is the motivator for our analysis. Expected future decline in the strength of the Atlantic Meridional Ocean Circulation (AMOC; Fox-Kemper et al.,

90 2023) will likely result in a declining ocean CO_2 uptake due to less transport of CO_2 enriched surface waters into the deep ocean. Projections indicate a reduced CO_2 uptake/sink in the global oceans correlating with a gradual reduction of the strength of the AMOC (McKinley et al., 2023; Liu et al., 2023). A slowing AMOC impacts ocean biology and solubility carbon pumps: CMIP5 analysis projects a weakening of the biological pump from surface waters with the largest decreases in effective CO_2 uptake under the strongest warming scenarios (Bopp et al., 2013; Fu et al., 2016; Laufkötter et al., 2016; Liu

95 et al., 2023). This is in part explained by ocean warming, which result in a decline in PP, also contributing to a decrease in

ocean CO_2 uptake in some regions (Kwiatokowski et al., 2020), however ocean warming and climate change also leads to sea ice decline, which results in increased PP regionally (Vancoppenolle et al., 2013). The projected climate driven impacts on the AMOC are yet not seen in the strength of regional components of the AMOC in the northern North Atlantic (Østerhus et al., 2019; Lozier et al., 2019; Orvik et al., 2022). Also, over the last two decades the estimated AMOC strength at 26°N is dominated by interannual to decadal variability with a marginal significant negative trend (Volkov et al., 2024). These findings underscore how variability in North Atlantic ocean and climate conditions, including fluctuations in AMOC strength, can modulate both the magnitude and regional distribution of oceanic CO_2 sinks.

We aim to understand the sensitivity and drivers of the atmosphere–ocean CO_2 flux in an ESM system on interannual and decadal timescales. Through our analysis we establish which predictors can explain the CO_2 flux variability in the five regions of the northern North Atlantic. We define regression models based on physical and dynamic predictors, to explore how well we can predict and understand future CO_2 flux variability.

1.1 Approach

The aim of this work is to understand how simulated interannual to decadal variability can help build confidence in future changes and a better understanding of uncertainties related to ocean processes and variability. We analyse ensemble data from 10 historical simulations with the EC-Earth3-CC global climate model with interactive ocean biogeochemical cycling. To assess the drivers of the interannual and decadal CO_2 flux variability in the northern North Atlantic we initially establish an overview of the relationship between the CO_2 flux variability and parameters that could potentially drive this variability across the northern north Atlantic and in defined sub regions (Fig. 1b).

Firstly, we use the gas transfer equations to check if we can reproduce the simulated CO_2 flux variability in the different regions from archived model data for the individual ocean region. Based on the gas transfer equation (Eq. 1-3) we expect SST, sea surface salinity (SSS), ΔpCO_2, wind and sea ice concentration (SIC) to be controlling physical parameters driving the simulated CO_2 flux variability. We additionally explore the relation of integral between CO_2 flux variability and parameters representing ocean dynamics or processes by including parameters such as mixed layer depth (MLD) and sea surface height (SSH), which are not direct drivers of atmosphere–ocean gas exchange. For each region, we integrate the CO_2 flux and define high and low CO_2 flux years for short and long timescales. We construct ensemble mean composite 2D maps of the CO_2 flux by subtracting the low flux years from the high flux years and by combining all ensemble members. We use the high and low flux years defined for the CO_2 flux to also construct composite maps of other key physical parameters.

Secondly, informed by the composite maps and identified controls of the CO_2 flux variablility, we define ten indexes that can be correlated with the CO_2 flux timeseries. The indexes are based on the parameters contributing to the gas exchange equations (Eq. 1-3) SST (AMO), SSS, wind and SIC, climatic modes of variability such as NAO, the ocean circulation strength (SSH index representing gyre circulation strength), MLD and AMOC. The specific definition of the different indexes and why we have chosen them is described in section 3. We have chosen to exclude ΔpCO_2 and other

Deleted: North Atlantic ocean and climate variability have the potential to modulate the magnitude of and regional patterns of CO_2 sinks.…

Deleted: ing

Deleted: B

Deleted: , however

Deleted: we also define and

Deleted: dynamic drivers

Deleted: as direct indicators of regional circulation changes

Deleted: at two

Deleted: o

Deleted: I

Deleted: , AMO, SIC variability, NAO, AMOC strength, wind variability, MLD and SSS variability,

Deleted: t

biogeochemical parameters, to focus our analysis on the physical processes and dynamical parameters affecting CO_2 flux variability.

150   Lastly, in order to understand how much of the CO_2 flux variability that can be explained and described by physical variables and indexes alone, we set up simple linear multivariable regression models for each region and discuss differences in explained variability across interannual and decadal timescales.

1.2 EC-Earth3-CC

155 EC-Earth3-CC is the carbon cycle (CC) version of the EC-Earth3. EC-Earth3 is an Earth system model, developed by the EC-Earth consortium (https://ec-earth.org), and contributes to the Coupled Model Intercomparison Project (CMIP). EC-Earth3 comprises several model components describing atmosphere, ocean, sea ice, land surface, dynamic vegetation, atmospheric chemical composition, ocean biogeochemistry and the Greenland Ice Sheet. EC-Earth3 (Döscher et al., 2022) consists of the atmosphere model IFS, land surface module HTESSEL and the ocean model NEMO3.6 (Madec 2015).

160   EC-Earth3-CC describes the carbon cycle and is used for the Coupled Climate-Carbon Cycle Model Intercomparison Project (C4MIP; Jones et al., 2016). The configuration allows for concentration driven simulations and with emissions forcings. The CO_2 flux is calculated from and proportional to the difference in partial pressure of (ΔpCO_2) between the atmosphere and the surface of the ocean (Döscher et al., 2022).

      EC-Earth3-CC runs with NEMO3.6 coupled to PISCES-v2 (Pelagic Interactions Scheme for Carbon and Ecosystem

165 Studies volume 2; Aumont et al., 2015), a biogeochemical model simulating marine biological productivity and the biogeochemical cycling of carbon and the main nutrients. Primary productivity is computed based on the availability of the main nutrients (P, N, Si, Fe), with a constant Redfield ratio (P : N : C = 1 : 16 : 122) (redfield ratio from Takashi et al., 1985; Aumont et al., 2015). Air-sea gas exchange for carbon dioxide is parameterised from Wanninkhof (1992), updated in Wanninkhof (2014) to Eq 1:

170
$$F = k\,K_0(pCO_{2w} - pCO_{2a}) \qquad\qquad (1)$$

where F is the flux (mass area^{-1} time^{-1}), k is the gas transfer velocity (lenght time^{-1}) and K_0 is the solubility (mass volume^{-1} pressure^{-1}), which is dependent on water temperature and salinity, pCO_{2w} and pCO_{2a} (pressure) are the partial pressures of CO_2 in equilibrium with surface water and the above lying air, respectively. The gas transfer velocity is dependent on wind speed according to Eq. 2:

175
$$k = 0.251\,U^2 \left(\frac{Sc}{660}\right)^{-0.5} \qquad\qquad (2)$$

where U is the wind speed (10 m height), Sc is the Schmidt number. The Schmidt number is dependent on water temperature. Furthermore, the CO_2 flux is dependent on the SIC in the region, as no exchange is allowed between the atmosphere and sea water across sea ice Eq. 3:

$$kgCO_2 = k'gCO_2 \times (1 - \%_{ice}) \qquad\qquad (3)$$

where kgCO2 is the atmosphere–ocean CO_2 flux after correcting for the SIC, k'gCO2 is the atmosphere–ocean CO_2 flux before correcting for SIC, $\%_{ice}$ is the concentration of sea ice which varies between 0 and 1 (Döscher et al., 2022, Aumont et al, 2015).

The present day (1982-2014) averaged air-sea CO_2 flux shows a general flux into the ocean in the North Atlantic and Nordic Seas (positive CO_2 flux, Fig 1a-c). Observations show a similar pattern of a positive flux (CO_2 uptake in the ocean) in the North Atlantic and Arctic region, and a negative flux (outgassing to the atmosphere) off the western coast of Africa across the Atlantic and off the coast of South America (Fig 1b). However, observations generally show a smaller air-sea CO_2 flux than simulated in EC-Earth3-CC (Fig 1c). Döscher et al. (2015) shows that the EC-Earth3-CC air-sea CO_2 flux is in general overestimated in the high northern latitudes (>50°N) in the northern hemisphere, and underestimated in the high latitudes in the southern hemisphere. However, the general distribution of the air-sea CO_2 flux is well represented in EC-Earth3-CC (Fig 1a-c).

The sea ice extent of EC-Earth3 (and therefore also EC-Earth3-CC) is in general overestimated in the Nordic Seas (NS) and NA compared to observations (Döscher et al., 2022; Tian et al., 2021). As no exchange between the atmosphere and seawater is allowed across sea ice in EC-Earth3, an overestimation of the sea ice extent will inevitably affect the CO_2 flux. The global pattern of the CO_2 flux and the overestimation of the sea ice extent emphasises the importance of sea ice and high latitude processes in the global climate system (Fig. 1).
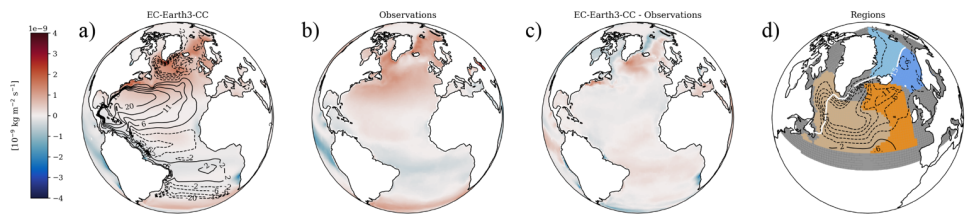
Figure 1: Atmosphere–ocean CO_2 flux averaged over the period 1982-2014 for a) EC-Earth3-CC, b) observation based reconstruction CO_2 flux data from Gregor and Fay (2021), c) their difference. Black lines show the mean barotropic streamfunction of the SPG circulation of ten ensemble members in Sv. Full line indicating positive values, dashed line indicating negative values. Closed dashed lines show the mean extent of the SPG. d) study regions: NA covering all regions (dark grey) SPW (beige), SPE (orange), NSE (blue), NS covering NSE as well (light blue), global average 15% SIC line (white contour) indicating the boundary between sea ice covered regions and sea ice free areas.

2. Data and methods

The analysis is based on EC-Earth3-CC historical runs 1850-2014 from all available ensemble members on ESGF (*https://aims2.llnl.gov/search/cmip6/*) (ten ensemble members: r1i1p1f1, r4i1p1f1, r6i1p1f1, r7i1p1f1, r8i1p1f1, r9i1p1f1, r10i1p1f1, r11i1p1f1, r12i1p1f1, r13i1p1f1). We make use of monthly mean fields of the parameters shown in Table 1. The data is preprocessed pointwise for analysis on two seperate timescales: decadal and interannual. For the decadal timescale a
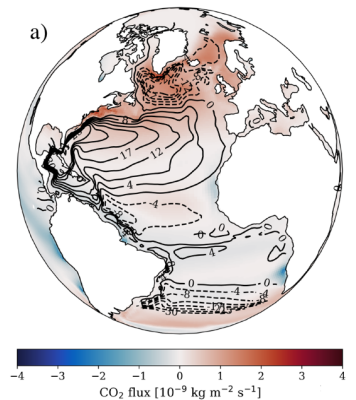
240 10 year low-pass filter (using CDO, filtering the data in the frequency domain: Schulzweida et al., 2012) has been applied to the data. Following the low-pass filtering the data has been linearly detrended to remove the anthropogenic forced changes due to increases in atmospheric greenhouse gases and to be able to focus on the internal climate and ocean variability of the North Atlantic. The atmosphere–ocean CO_2 flux (and ΔpCO_2) shows a modest linear increase from 1850–1950 and then a transition to a steeper increase until 2015 (see also section 2.2, Fig. 2). Therefore, in this case a two step piecewise linear fit

245 has been used to detrend the dataset. The model dataset has been detrended along the time axis for every grid cell, allowing for analysing the detrended data on a regional scale. Other parameters have been detrended using a linear fit. We choose not to apply any detrending to the streamfunction data at grid point level. A second preprocessed dataset of interannual variability is prepared by subtracting the low-pass filtered timeseries from the original model data. Also here, the interannual CO_2 flux and ΔpCO_2 dataset has likewise been detrended using a two-step linear fit, and other parameters using a linear fit.

250

Table 1

Parameters from EC-Earth3-CC

Parameter	Output variable name	Form of detrending	Unit
CO_2 flux	fgco2	two-step linear	kg m^{-2} s^{-1}
ΔpCO_2	dpco2	two-step linear	Pa
Sea surface temperature (SST)	tos	linear	°C
Sea surface salinity (SSS)	sos	linear	
Wind	sfcWind	linear	m s^{-1}
Mixed layer depth (MLD)	mlotstmax	linear	m
Sea surface height (SSH)	zos	linear	m
Sea ice concentration (SIC)	siconc	linear	%
Pressure at sea level	psl	linear	Pa
AMOC	msftyz	None	kg s^{-1}
Barotropic mass streamfunction	msftbarot	None	kg s^{-1}

2.1 Regions

This study looks into the CO_2 flux variability in multiple regions in the North Atlantic (Fig. 1b), to investigate the regional differences in the relationship between the CO_2 flux and the physical and dynamical processes. The geographic regions are defined considering the model representation of oceanographic domains. The North Atlantic (NA) region covers all of the

255 ocean in the region 40°N - 90° N, -78°W - 45° W, with avereage ocean CO_2 uptake. The Nordic Seas (NS) is defined roughly where warmer subpolar North Atlantic waters in the model meets waters of the Nordic Seas at the latitude of the

Greenland Scotland Ridge and defined as the region 60°N - 90° N, 28°W - 18°W. The Nordic Seas east (NSE) is defined as the NS, but only where model climatology has less than 15% sea ice and as such, representing the sea ice free part of the NS, allowing for unbiased investigation of the dynamics not related to the overestimated sea ice extent. The Subpolar region of the North Atlantic is divided into two oceanic domains: the Subpolar West (SPW) and the Subpolar East (SPE). The SPW is defined as where the annual mean SSS is <34.2 within the region 45°N - 60°N, 52°W -10°W, the part of the subpolar gyre recirculating watermasses modified by low salinity polar outflow and melting sea ice. The SPE is defined as SSS >34.2 within the region 45°N - 64°N, 52°W - 10°W in the path of the North Atlantic current. The SPE, like the NSE, represents a region with no sea ice cover (climatological SIC <15%).

2.2 CO_2 flux variability

Table 2

Variability (standard deviation, std) of ensemble mean CO_2 fluxes for F (model output), F_{calc} (calculated flux) in interannual (int) and decadal (dec) timescales

Std	F [10^{-11} kg m^{-2} s^{-1}]		F_{calc} [10^{-11} kg m^{-2} s^{-1}]		Area of region [10^{12} m^2]
	Int	Dec	Int	Dec	
NA	3.22	2.16	2.92	2.39	11.27
NS	5.35	5.87	5.05	5.56	0.96
NSE	8.23	6.99	7.08	5.93	0.27
SPW	8.22	5.49	7.52	5.28	2.86
SPE	6.85	5.84	5.96	4.97	1.04

Archived climate model data available from CMIP6 on the ESGF nodes typically consists of monthly mean fields of physical, biological and chemical parameters. This includes surface air sea CO_2 fluxes from EC-Earth3-carbon cycle as well as ocean properties. The reproducibility of simulated integrated fluxes (F) derived from other parameters (Eq. 1-3), particularly their variability across different timescales, provides a useful benchmark. It sets an upper limit on how much of the model variability we can expect to explain using physical quantities from archived monthly-averages data. Figure 2 also shows the time evolution of F_{calc} (CO_2 flux calculated according to Eq 1-3) of a selected ensemble member (r4i1p1f1) and for the NS, NSE and SPE region only. To accurately reproduce the simulated flux, F_{calc} is computed using a scaled wind speed. Since F_{calc} is derived from monthly mean values of all parameters, some of the short-term variability in dynamic factors—particularly wind speed—is smoothed out, leading to a lower mean wind speed compared to the daily mean used in EC-Earth3-CC. Hughes et al. (2012) discusses a averaging-related bias linked to ocean surface flux calculations and show that the use of monthly mean fields can introduce a bias into the mean flux estimates (also discussed by Esbensen and Reynolds, 1981; Simmonds and Dix 1989; Gulev, 1994; 1997; Josey et al., 1995; Zhang 1995; Esbensen and McPhaden 1996; Simmonds and Keay 2002). Given that

Deleted: typically

Deleted: The level of reproducibility of simulated integrated fluxes from other parameters (Eq. 1-3) (F) and in particular their variability across time-scales from archived averaged monthly data will constitute an upper limit for our ability to explain from physical quantities the model variability.

Deleted: is

Deleted: integrated

Deleted: a

Eq. 2 shows a nonlinear dependence of CO_2 flux on wind speed (U^2), even small-scale wind variability can have a significant impact on flux calculations. To account for the reduced wind variability in the monthly mean fields and ensure consistency with the original flux calculation, a scaling factor of 1.2 is applied to the wind speed when computing F_{calc}. The scaled wind is only used for this calculation and not in any of the other analyses. It is also expected that the CO_2 flux variability is dependent on SST and SSS variability, however the effect of SST and SSS on the solubility constant (K_0) is too small to be considered important in these calculations, and the SST and SSS components of Eq 1-3 is therefore not scaled. The absolute level of the F_{calc} compared to the model flux is well captured including the trend. For this ensemble, the correlation between the estimated flux and the model output in SPE exceeds 0.9 (R^2) with a regression factor close to unity (1.1). We find comparable/significant skill in reproducing fluxes for the shorter timescale (not shown).

Figure 2 shows the average (weighted mean) CO_2 flux time series F for each region with interannual variability removed. The anthropogenic trend is evident in all regions including the accelerated trend after 1950. Differences between regions are evident with NSE showing the largest CO_2 uptake per unit area. Strong decade-scale variations do modulate regionally the accelerated trend after 1950 emphasizing the importance of ocean variability. Removing the anthropogenic trend and isolating interannual and decadal variability reveals i) relatively comparable levels of variability across regions and ii) a stronger variability on short timescales (Table 2). Ensemble mean results indicate that NSE, which is also the smallest area, is subject to strongest variability on both timescales, followed by the SPW (Table 2).
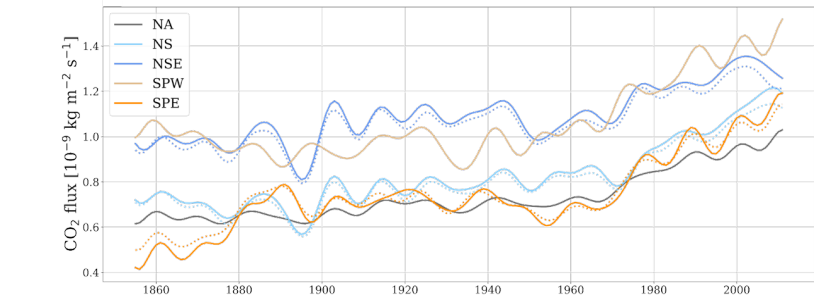
Figure 2: Decadal variability in the simulated CO_2 flux (F, solied line) and calculated flux (F_{calc}, dotted line) for ensemble member r4i1p1f1. Here the weighted mean is shown to compare the fluxes and variability across regions. F_{calc} only showed for NS, NSE, SPE

3. Results

3.1 Regional CO_2 flux variability

To visualise the patterns of CO_2 flux variability across timescales and regions, we create composite maps of the CO_2 flux and the parameters we expect to be important drivers of the variability. These parameters include parameters already presented above (SST, SSS, SIC, ΔpCO_2 and wind), however for the next part of the analysis we add mixed layer depth (MLD) and sea

surface height (SSH). These parameters represent larger scale dynamics such as ocean circulation (SSH, gyre strength) and

330 vertical mixing (MLD), which are candidates to be indirect processes controlling the CO_2 flux variability in EC-Earth3-CC. After detrending the data as described above, we define high and low CO_2 flux years in the different study regions based on the mean standard deviation for all the ten members (+/-) one std from the regional mean. The years are defined and selected for each member for all the parameters, where after the difference of the ensemble mean high minus low flux years is shown in composite maps (Fig. 3-7).

335 The North Atlantic region covers all the other regions. The CO_2 composite maps show a widespread homogeneous pattern of CO_2 uptake, intensified across the subpolar region (Fig. 3) and with regional differences. This includes the Irminger and Iceland Basins, where fluxes are moderated and locally reversed. On decadal timescales, positive values (increased CO_2 uptake) are confined to areas near the sea ice edge indicating that this exerts significant control over North Atlantic average CO_2 flux variability at longer timescales (Fig. 3b). On interannual timescale, the widespread CO_2 uptake

340 mirrors a widespread pattern of stronger winds and colder SST, indicating that these parameters are potential drivers of the CO_2 flux variability on shorter timescales. This is not the case for decadal variability where only positive wind speed project on regions of enhanced CO_2 flux, temperature generally warm and act to reduce solubility. A positive ΔpCO_2 pattern compares spatially with the positive CO_2 flux anomaly and negative SST anomaly (Fig. 3a). On the decadal timescale, a negative SSH anomaly, indicating a strengthening of the subpolar gyre, compares spatially with the positive CO_2 flux

345 anomaly in the subpolar gyre region, which suggest that the strength of the subpolar gyre also could be a potential dynamical driver of the CO_2 flux variability, modifying key parameters like SST and SIC. The CO_2 flux variability pattern in the North Atlantic appears relatively homogenous, while its comparisons with other parameters are less distinct, except for SST on short timescales and SIC on long timescales. This suggests that multiple dynamics may be influencing CO_2 flux variability. To better understand these influences, we will analyse smaller, well-defined regions to identify the key drivers of CO_2 flux

350 variability.

355

North Atlantic

365
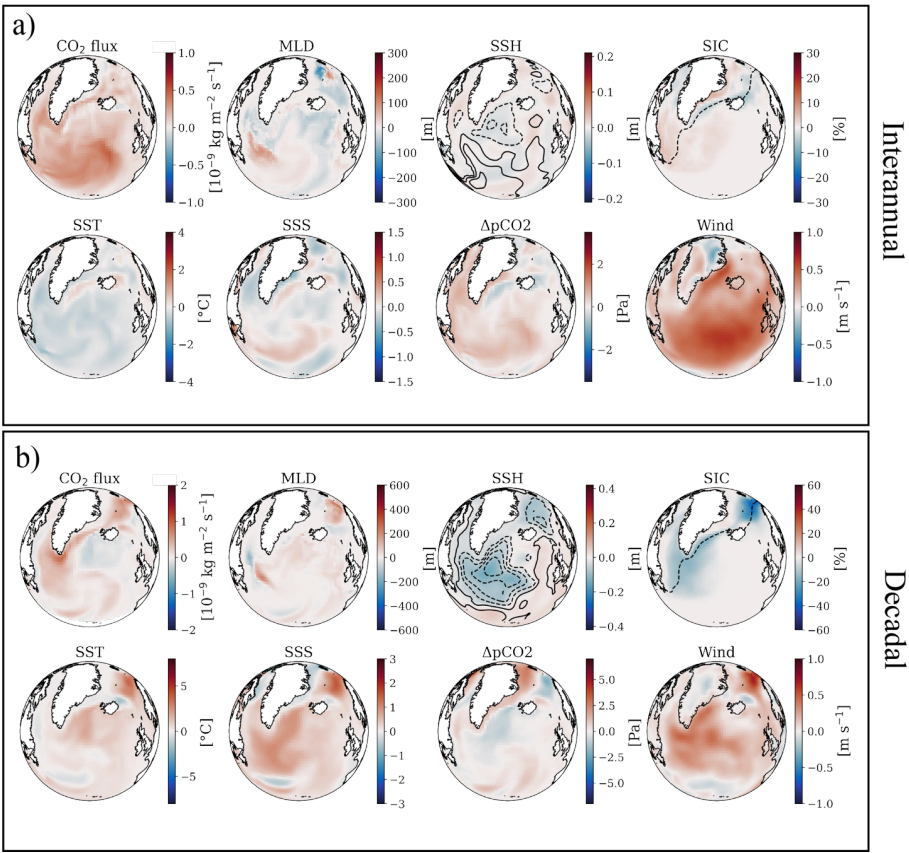
Figure 3 Anomalies of the high-low years of the dynamic parameters compared to the CO_2 flux anomaly in the NA. a) showing interannual timescale and b) showing decadal timescale. Full and dashed lines on top of the SSH anomaly shows the barotropic mass streamfunction anomaly and dashed line on top of SIC anomaly shows the 15% SIC climatology (mean of ten ensemble members on both timescales).

370   Focusing in on the the Nordic Seas region, we see a widespread and homogeneous pattern of CO_2 uptake on interannual timescale (Fig. 4), on short timescales confined to the Nordic Seas emphasising the role of regional dynamical systems and need for a regional analysis. The Nordic Seas shows the strongest flux anomalies across all the regions, in particular on long timescales. On decadal timescales, the CO_2 uptake is confined to an area of varying SIC in the Nordic Seas with dynamical

consistent patterns also in the SPG region, indicating that SIC is the main driver of the CO_2 flux variability in this region on longer timescale (Fig. 4a). Positive SST anomalies reaching 5°C on decadal scale would counteract the effects of sea ice variability. On the shorter timescale, the CO_2 uptake is enhanced across most of the Nordic Seas region, however, on decadal scale a small part of the region shows CO_2 outgassing (Fig. 4b), likely linked to the strong warming of the composite and reduced ΔpCO_2. Again, the positive CO_2 flux anomaly is perfectly confined to areas within an area of decrease in SIC, indicating that SIC is the main driver of CO_2 flux variability on the shorter timescale as well. The decrease in SIC is greater in the Nordic Seas composite maps compared to the North Atlantic maps. On both timescales stronger winds compare spatially with the increased CO_2 uptake, similar to the North Atlantic region. However, the wind anomaly is stronger on the longer timescales compared to the shorter timescales. Following a decrease in SIC we see a deepening of the MLD due to increased convection, increasing the mixing and allowing for an increase in air-sea CO_2 flux. However, the small scale and spatial pattern associated with enhanced mixing is not obviously reflected in the patterns of CO_2 uptake. Also, from the spatial comparison of patterns, it is clear that ΔpCO_2 changes alone cannot explain the CO_2 flux variability.
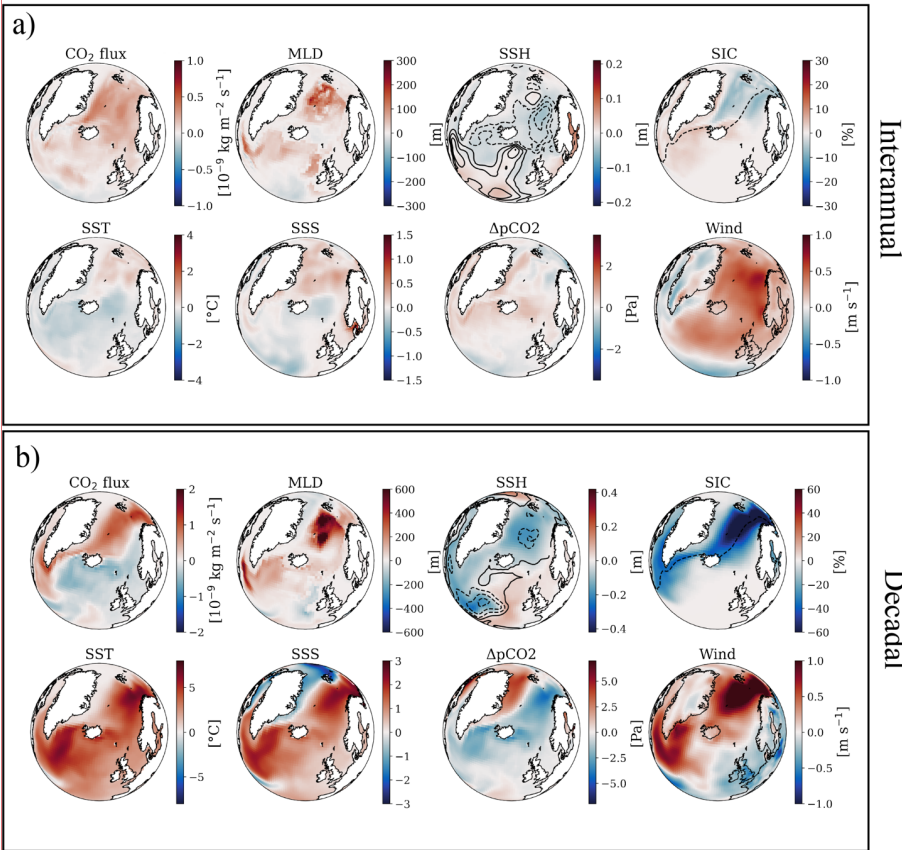
390   **Figure 4 Anomalies of the high-low years of the dynamic parameters compared to the CO$_2$ flux anomaly in the NS. a) showing interannual timescale and b) showing decadal timescale. Full and dashed lines on top of the SSH anomaly shows the barotropic mass streamfunction anomaly and dashed line on top of SIC anomaly shows the 15% SIC climatology (mean of ten ensemble members on both timescales).**

395   The Nordic Seas East region represents the sea ice free part of the Nordic Seas (less than 15% SIC) and is in the path of the North Atlantic current crossing the Greenland Scotland Ridge. The composite maps of high minus low CO$_2$ flux years show an increased CO$_2$ uptake (Fig. 5) confined to the NSE region highlighting that our regionalisation is relevant and allow us to
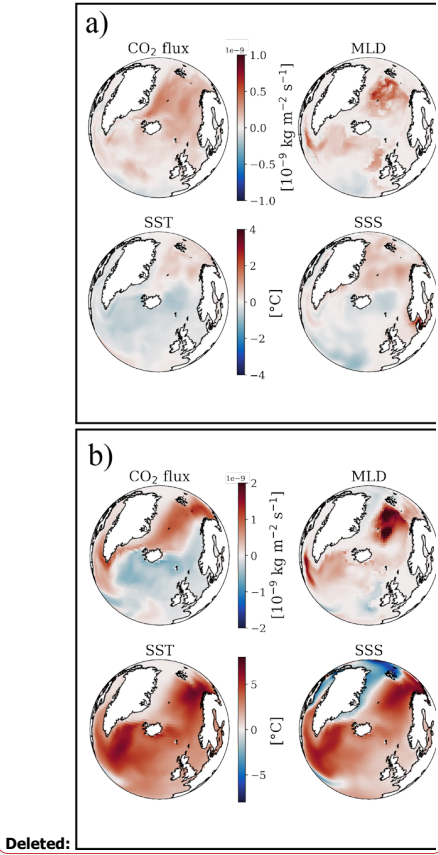
400 isolate a dynamical regime. The region is confined by the 15% SIC line, and shows a widespread positive CO_2 flux anomaly. Figure 5a illustrates that the interannual variability shows an increase in wind which compares spatially with a deepening of the MLD and an increase in the air-sea CO_2 flux. These patterns are more pronounced for the NSE than for the NS region. A decrease in SSH indicates a strengthening of the Nordic Seas gyre circulation, the eastern part, mirroring an increase in MLD and CO_2 flux indicating a dynamic driver of the CO_2 flux variability. Figure 5b shows a confined pattern of CO_2 uptake,

405 which compares spatially with a confined pattern of stronger wind, increased MLD as a result of a strengthening of the Nordic Seas Gyre (NSG; shallowing of the SSH) and increased SSS. Compared to the North Atlantic region, the Nordic Seas East gives a clearer indication of the driving forces behind the CO_2 flux variability.
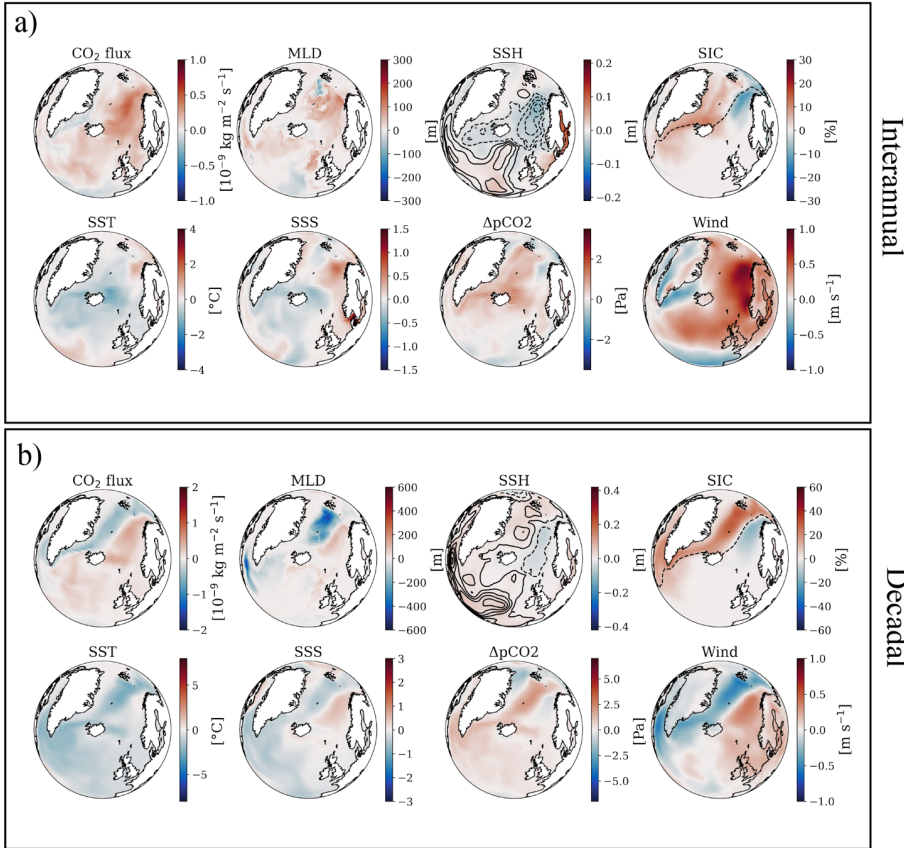
Figure 5 Anomalies of the high-low years of the dynamic parameters compared to the CO₂ flux anomaly in the NSE. a) showing interannual timescale and b) showing decadal timescale. Full and dashed lines on top of the SSH anomaly shows the barotropic mass streamfunction anomaly and dashed line on top of SIC anomaly shows the 15% SIC climatology (mean of ten ensemble members on both timescales).

In the western part of the subpolar region, the CO₂ flux spatial pattern is strikingly similar to the pattern we can construct for the entire North Atlantic on both timescales (Fig. 3 and 6). This can in part be expected from the vast area of the region hereby dominating the area-averaged fluxes and composites. Key differences with the NA region includes the Irminger Sea where also SSH patterns indicate a dynamical separation on interannual scales. On the interannual timescale the region
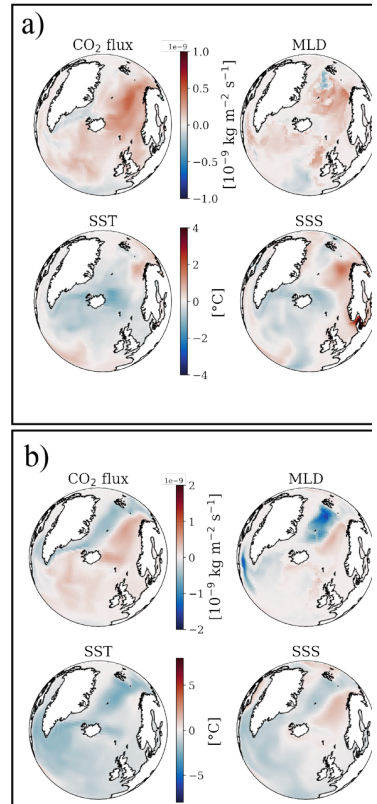
shows CO_2 uptake within the full region (Fig. 6a), whereas the decadal CO_2 flux shows both positive and negative anomalies within the region (Fig. 6b). In general all the parameters show similar patterns to the North Atlantic on both timescales. However, on the interannual timescale we see a more clear and confined signal from SST and SSS compared to the North Atlantic. A negative SST anomaly compares spatially with increased CO_2 uptake in the full region, whereas a positive SSS anomaly in most of the region shows a relationship with the CO_2 flux variability, emphasising how the SSS can work as an indirect driver or indicator. On the decadal timescale we see a clear and confined signal in the indicated drivers of the CO_2 flux compared to the North Atlantic region. Here, we see that the CO_2 uptake is confined within the region of decreasing SIC, indicating that SIC forces a main control on the CO_2 flux variability in the region. Furthermore, we see a greater strengthening of the subpolar gyre as indicated by the decrease in SSH on both timescales, however the strongest signal is seen on the longer timescale, where we also see a shift towards the east as expected in a strong SPG phase. The strengthening of the subpolar gyre results in a deepening of the MLD and introduces more saline Atlantic Water into the system from further south, which explains why we see a positive SSS anomaly and increased CO_2 uptake. As in the North Atlantic region, we see opposite anomalies for the SST on the two timescales. A negative SST anomaly mirrors a positive CO_2 flux anomaly on the short timescale, whereas on the longer timescale, we see a positive SST anomaly and a positive CO_2 flux anomaly.

Subpolar West
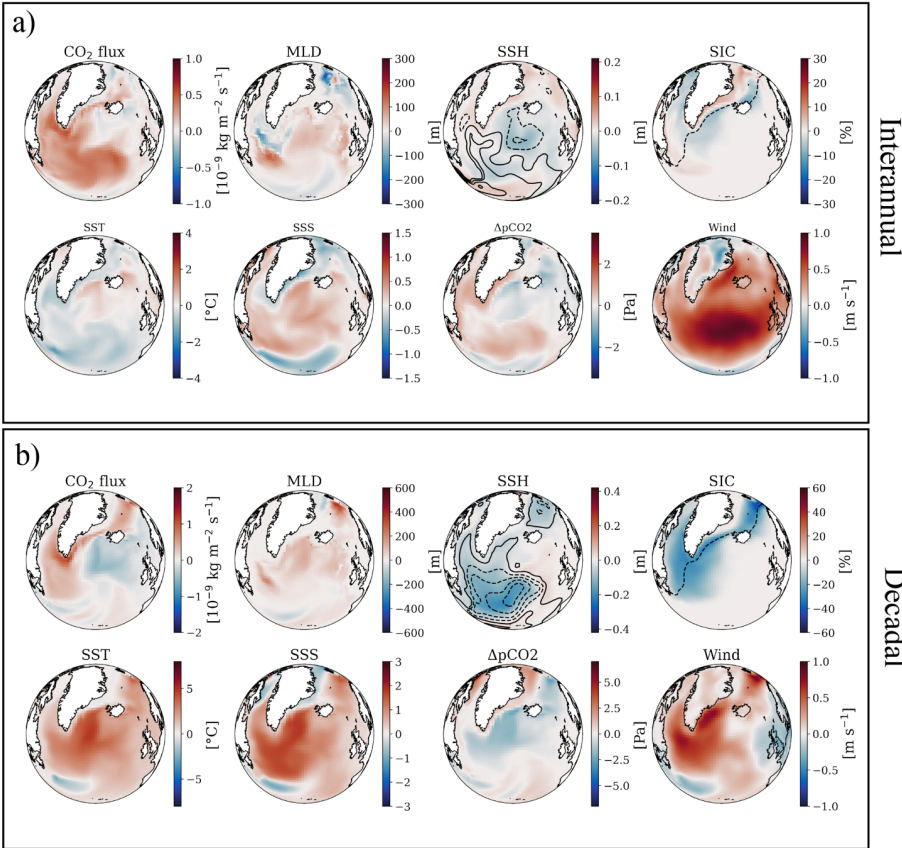
Figure 6 Anomalies of the high-low years of the dynamic parameters compared to the CO₂ flux anomaly in the SPW. a) showing interannual timescale and b) showing decadal timescale. Full and dashed lines on top of the SSH anomaly shows the barotropic mass streamfunction anomaly and dashed line on top of SIC anomaly shows the 15% SIC climatology (mean of ten ensemble members on both timescales).

450
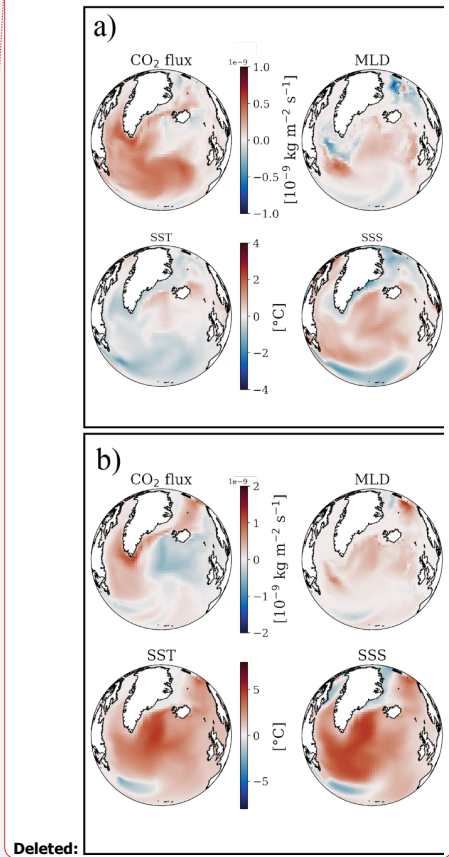
455   Lastly, we look at the eastern part of the subpolar region (Fig. 7). The composite maps show patterns of increased CO_2 uptake, which is regionally well confined to the eastern subpolar gyre and not apparently analogue to the composite patterns derived for SPW. This includes also the North Atlantic region. On the interannual timescale SSH reflects what may best be characterized as a relative blocking of the path of the North Atlantic current (a closed gyre system building up sea surface height). On the decadal timescale this blocking cell is located further south, outside of the SPE region, but in both cases

460   result in cooling of the wider subpolar region as well as freshening. Despite these basin wide linkages, the CO_2 flux changes are regionally exaggerated in the SPE. Not surprisingly, the dynamical changes – a blocking of the path of the North Atlantic current – are also characteristic of the composite maps for the NSE region (Fig. 5). Despite this apparent similarity, the CO_2 flux patterns are in both cases not extending across the Greenland Scotland Ridge. This may be explained by phase differences in the impacts.

465   The spatial pattern of positive CO_2 flux anomaly reflects a shallowing of the MLD on the interannual timescale. This cannot directly be linked to increased uptake, on the contrary as described in section 1 and 3.1, as a shallowing of the MLD is related to a less ventilated water column, and thereby a decrease in the CO_2 uptake. This link is discussed further in the next section. Also on the interannual timescale, a positive wind anomaly, and a negative SST and SSS anomaly also align spatially with positive CO_2 flux anomalies. On the decadal timescale, the signal from the MLD and wind is less clear,

470   however, a negative SST and SSS anomaly compares spatially with the increased CO_2 uptake in the region.
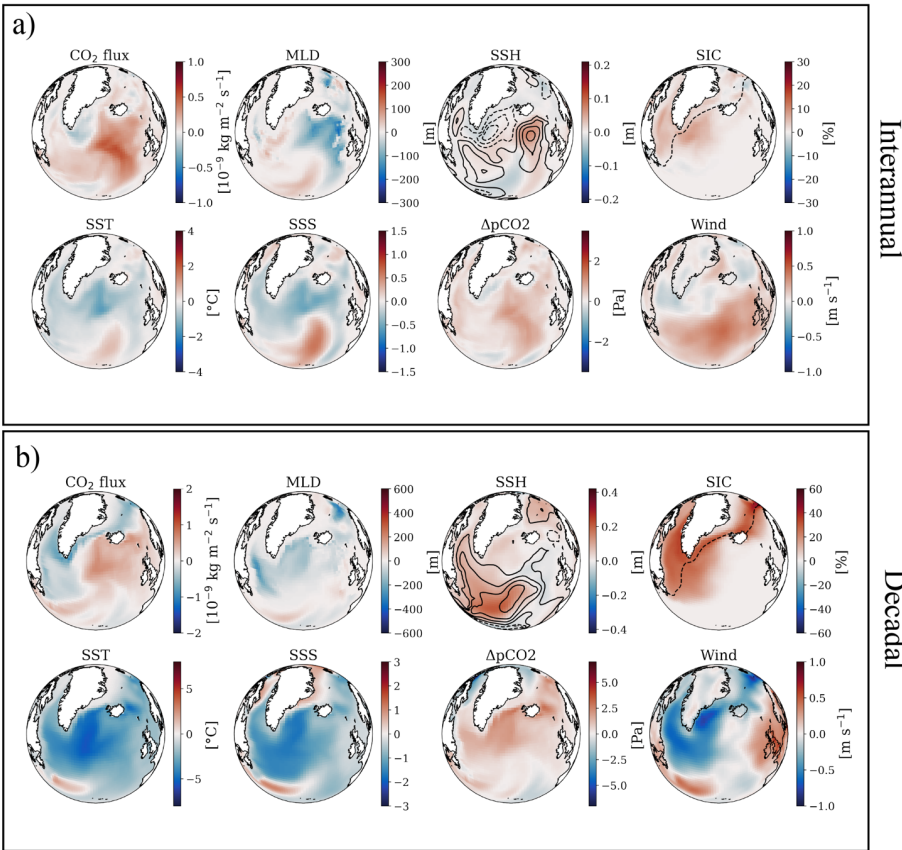
Figure 7 Anomalies of the high-low years of the dynamic parameters compared to the CO₂ flux anomaly in the SPE. a) showing interannual timescale and b) showing decadal timescale. Full and dashed lines on top of the SSH anomaly shows the barotropic mass streamfunction anomaly and dashed line on top of SIC anomaly shows the 15% SIC climatology (mean of ten ensemble members on both timescales).

485
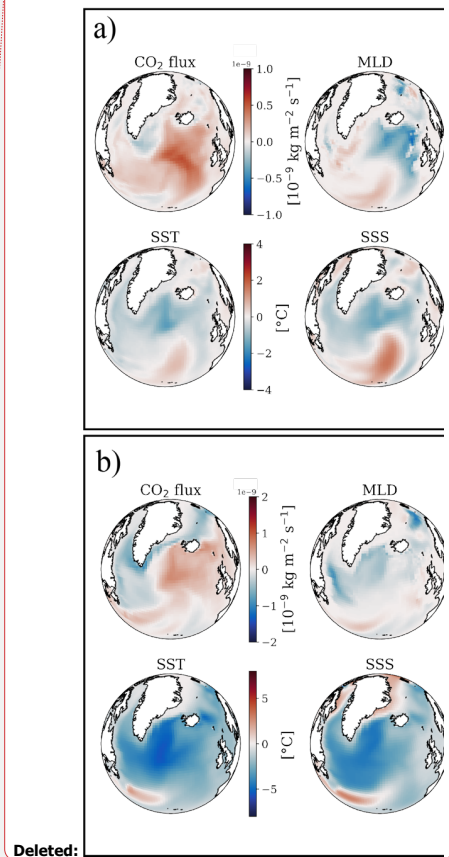
3.2 Ocean indexes

490 Following the qualitative discussion of the relationship between the CO_2 flux variability and the dynamical parameters on different timescales, we define integrated quantities and make use of ocean indicators such as the subpolar gyre index to understand statistical significance of the identified relationships between the CO_2 flux and ocean variability (Table 3).

The Subpolar Gyre index (SPGi) is here defined simply as the minimum SSH of the NA region. This differs from other definitions (Hátún et al. 2005, Berx and Payne et al., 2017) but captures the main variability of the Earth System Model

495 analysed. The index is inverted, meaning that a positive (negative) anomaly indicates a strong anticyclonic (weak) SPG. The subpolar gyre index describes not only the state of the subpolar region but from observations also shown to characterize variability in water mass properties at the gateways to the Nordic Seas (Hátún et al., 2005; Hátún et al 2017). As such, the SPGi may be linked to CO_2 flux variability directly by describing the extent of the characteristic colder and fresher subpolar upper ocean water masses and indirectly through correlations with other drivers such as variability in sea-ice margins, wind

500 stress and ocean mixing locally and remote (Nordic Seas). From correlation coefficients (zero lag) between the SPGi with the CO_2 flux anomaly for the different regions (NA, NS, NSE, SPW, SPE), presented in Table 3, it is clear that the SPGi does not explain the CO_2 flux variability on the interannual timescale very well, though reassuringly the highest correlation are found for the SPW region. The SPGi correlates better on the decadal timescale, with an ensemble mean of 0.31 and 0.44 in the NA and SPW respectively. Several ensemble members show a correlation coefficient of 0.4 or higher in both regions,

505 but a few ensemble members show very low correlation, resulting in reduced ensemble mean values. The SPE shows a large spread in individual ensemble correlations with both positive and negative correlations, resulting in an ensemble mean of -0.24 and -0.17 (interannual and decadal, respectively). The low degree of correlation on both timescales is expected in part due to the finding from the composite map analysis of a more regional SSH (and streamfunction) 'blocking pattern' of the North Atlantic Current.

510 The Nordic Seas Gyre index (NSGi) is defined as the minimum SSH in the NS region, similar to the SPGi. The index is inverted, meaning that a positive value indicates a strong anticyclonic gyre circulation, whilst a negative value indicates a weakening of the gyre circulation. The NSGi will be modulated by changes in wind stress curl and also not independent of other possible indices defined on the basis of MLD and SIC. We have no a-priori expectation of a strong relation between the NSGi and CO_2 flux in other regions. The NSGi correlates well with the CO_2 flux variability in the NS

515 on the decadal timescale (0.54, Table 3), but also on the interannual timescale (0.30, Table 3). A strong (weakened) NSGi results in an increased (decrease in) CO_2 uptake in the ocean. Hátún et al. (2021) shows that a strong NSG circulation results in an uplifted thermocline, which results in more ventilation of deeper water. The ventilation of deeper water could lead to an increased air-sea CO_2 flux, and work as a driver for the increased CO_2 uptake in the NS. The composite maps show a strengthening of the NSG (deepening of the SSH) on both timescales, however a greater strengthening on decadal timescale,

520 indicating that a strengthening of the NSG could result in an increased atmosphere–ocean CO_2 flux.

The AMO index is defined as the anomaly of the mean SST in the NA region. For the regions within the NA, the index is defined as a SST index, which is the anomaly of the mean SST within the region. We have chosen to use the SSTi for the smaller regions, to investigate the direct relationship of SST and CO_2 flux variability within the regions. A positive AMO/SSTi phase describes a warming of the North Atlantic. As higher SST's increase the pCO_2 in the ocean due to lower solubility, the AMO should be negatively correlated to the CO_2 flux. However, Breeden and McKinley (2016) shows how a positive AMO phase results in a decrease in DIC in the SPG, which decreases the solubility and increases the fCO_2 (and the pCO_2). On the decadal timescale we see that the CO_2 flux variability in NS and SPW region correlates positively (0.36 and 0.29, Table 3) with the SSTi, which can be related to the dynamics explained by Breeden and McKinley (2016). Also, an increase in temperature in the NS would result in a decrease in SIC, allowing for an increase in CO_2 flux. Breeden and McKinley (2016) states that SST and the solubility of CO_2 in the ocean still affects the pCO_2 in the ocean (and thereby the air-sea CO_2 flux), but that the biogeochemical dynamics, such as DIC are of a stronger amplitude. The NSE and SPE regions shows an inverted correlation between the CO_2 flux variability and the SSTi on both timescales (NSE: -0.12 and -0.41 SPE: -0.15 and -0.38, interannual and decadal), indicating that the temperature effect on the CO_2 solubility in the surface ocean dominates the CO_2 flux variability in these regions (Table 3). In the NA the degree of correlation varies a lot between the ensemble members from a negative/weak correlation to a stronger correlation, which makes it difficult to say anything in general about the full NA region.

The sea ice index (SIi) is defined as the SIC anomaly in the specified regions. An increase in SIC results in a decrease in CO_2 flux into the ocean in case no other factors are changing. In the NS the SICi in general has a strong negative correlation with the decadal CO_2 flux anomaly, all of the members showing a correlation coefficient above 0.50, resulting in an ensemble mean of -0.64 (Table 3). The interannual variability in the NS shows a lower correlation, with an ensemble mean of -0.36 (Table 3). On both timescales, the SPW region shows a weaker negative correlation compared to the NS (-0.04 and -0.36, interannual and decadal), as expected due to a smaller degree of sea ice extent in the SPW. However, it is clear that the SIC is still dominating the CO_2 flux variability in this region. The NA region shows the weakest correlation between the SICi and the CO_2 flux variability, which migth be explained by the fact that the sea ice covered region of the NA is small (-0.02 and -0.26 interannual and decadal). The SICi has not been applied to the NSE and SPE regions, as they are more or less sea ice-free.

The NAO index is defined as the atmospheric surface pressure level anomaly between Iceland (65° N, 20° E) and the Azores (40° N, 25° E) in the winter months (djfm; Hurrel 1995). The correlation between the NAO and CO_2 flux is in general strongest on the interannual timescale, showing a correlation coefficient of around 0.3 for most regions, except SPE that shows 0.12 and 0.35 interannual and decadal, respectively. On the decadal timescale the ensemble mean correlations are weaker, however in particular in the ice-free SPE and NSE and in the NA some ensemble members show a correlation of 0.4-0.5 (Table 3). The NAO and associated wind stress and wind stress curl impacts the ocean dynamics of the region including sea ice distribution which may explain the positive correlations, whereas the direct effects of changes in wind stress on gas transfer would be expected to result in negative correlations for some regions.

The AMOC index (AMOCi) is defined as the anomaly of the maximum of the model Atlantic Meridional Overturning Circulation (streamfunction) at 45°N in the top 1000m of the water column.We choose 45°N to align with the boundary of the Subpolar and subtropical gyres and reduce potential time lag, that would follow from using an index defined at lower latitudes. On the interannual timescale, the AMOCi shows a strong negative correlation in the NA and SPW regions (-0.40 and -0.47, Table 3), indicating that a weakened AMOC resulting in less heat transport to the Northern North Atlantic will result in increased ocean CO_2 uptake. In the other regions, the ensemble members show a low correlation on the short timescale. On the decadal timescale, somewhat surprisingly, the AMOCi is not as closely and directly related to surface CO_2 exchange with both negative and positive correlation coefficients in all the regions, resulting in a weak average correlation (Table 3).

The wind index (Wi) is defined as the anomaly of the average near surface (10 m) wind speed in the different regions. As expected based on Eq. 2, the Wi correlates positively with the CO_2 flux variability for all regions independent on timescale. On both interannual and decadal timescale, the Wi shows a high correlation with the CO_2 flux in the NA (0.68 and 0.45), NS (0.73 and 0.70) and NSE (0.72 and 0.57, Table 3). However, SPW only shows a high correlation on an interannual timescale (0.80 and 0.26 decadal), whereas SPE shows a weaker correlation on both timescales (0.24, 0.26). In the composite maps all the regions show a strong positive wind anomaly, whereas the SPE region shows a weak positive anomaly on the interannual timescale and a mix of negative and positive anomalies on the decadal timescales, which might explain the weak correlation seen in the region.

To understand the dynamic process of upper ocean mixing and its effect on the atmosphere–ocean CO_2 flux variability a MLD index (MLDi) is defined based on the anomaly of the MLD max value of the regions. The MLDi shows a strong negative correlation in the SPE (0.53 interannual; 0.29 decadal, Table 3) on both timescales, and a strong positive anomaly in the NS (0.38 interannual, 0.57 decadal) indicating a complex, indirect and regionally different linkage. Spatial patterns of MLD show some resemblance to ΔpCO_2 in the SPE with an inverse relation (Fig. 7), which can be explained by shoaling of the mixed layer leading to less ventilation of DIC rich deeper layers and thus increased ΔpCO_2.

Salinity directly, but weakly influence the gas transfer (Eq. 1), but we choose to define also a SSS index (SSSi) as preliminary analysis showed a clear correlation between PP and SSS in the EC-Earth3-CC output data which can be exploited to be able to use the analysis from this study on different ESMs that might not include a biogeochemical component in possible future studies. Furthermore, the SSS dynamics also translates to the strength of the SPG, the melting of sea ice and transports of different water masses in the North Atlantic. We have defined the SSSi as the SSS anomaly in the different regions. The SSSi shows the strongest interannual correlation in the SPW (0.33), and the strongest decadal correlation in the NS (0.52) and SPW (0.39). In the composite map of the NS region, we see a strong positive SSS anomaly correlating with a positive CO_2 flux anomaly (Fig. 4). The SSSi shows a strong negative correlation with the CO_2 flux in the SPE, which is also evident in the composite maps (Fig. 7).

Deleted: s
Deleted: n
Deleted: and
Deleted: a
Deleted: '

Table 3
Index analysis. Correlation coefficients are the mean of 10 ensemble members in interannual (int) and decadal (dec) timescales. In cursive min and max values for individual members are shown to indicate spread (uncertainty) of the index analysis. In bold parameters used for regression models in section 3.3.

	Corr. Coeff.	NA Int	NA Dec	NS Int	NS Dec	NSE Int	NSE Dec	SPW Int	SPW Dec	SPE Int	SPE Dec
SPGi	mean	0.04	**0.31**					0.21	0.44	-0.24	-0.17
	min	*-0.16*	*0.08*	-	-	-	-	*-0.01*	*0.18*	*-0.42*	*-0.71*
	max	*0.16*	*0.69*					*0.25*	*0.80*	*0.05*	*0.27*
NSGi	mean			0.30	0.54	0.25	**0.49**				
	min	-	-	*0.13*	*0.41*	*0.11*	*0.31*	-	-	-	-
	max			*0.53*	*0.76*	*0.40*	*0.66*				
AMO /SSTi	mean	-0.27	0.19	0.09	0.36	**-0.12**	-0.41	**-0.25**	**0.29**	**-0.15**	**-0.38**
	min	*-0.46*	*-0.13*	*-0.05*	*0.03*	*-0.39*	*-0.64*	*-0.42*	*-0.33*	*-0.31*	*-0.83*
	max	*-0.04*	*0.56*	*0.28*	*0.59*	*0.19*	*-0.24*	*-0.12*	*0.64*	*0.03*	*0.38*
SICi	mean	-0.02	-0.26	**-0.36**	**-0.64**			-0.04	-0.36		
	min	*-0.09*	*-0.49*	*-0.51*	*-0.84*	-	-	*-0.09*	*-0.68*	-	-
	max	*0.08*	*0.07*	*-0.17*	*-0.54*			*0.13*	*-0.29*		
NAO	mean	0.30	0.24	0.29	0.18	0.35	0.31	0.30	0.13	0.12	0.35
	min	*0.17*	*0.02*	*0.20*	*-0.09*	*0.24*	*0.14*	*0.19*	*-0.19*	*-0.09*	*0.11*
	max	*0.46*	*0.47*	*0.37*	*0.30*	*0.44*	*0.45*	*0.46*	*0.30*	*0.32*	*0.57*
AMOCi	mean	**-0.40**	0.20	0.11	0.26	0.17	**-0.06**	**-0.47**	0.16	-0.20	0.02
	min	*-0.53*	*-0.08*	*-0.06*	*0.02*	*0.05*	*-0.33*	*-0.54*	*-0.21*	*-0.33*	*-0.42*
	max	*-0.32*	*0.49*	*0.28*	*0.47*	*0.34*	*0.14*	*-0.37*	*0.42*	*-0.12*	*0.45*
Wi	mean	**0.68**	**0.45**	**0.73**	**0.70**	**0.72**	**0.57**	**0.80**	0.26	**0.24**	0.26
	min	*0.57*	*0.26*	*0.66*	*0.57*	*0.59*	*0.40*	*0.71*	*0.17*	*0.04*	*0.01*
	max	*0.78*	*0.56*	*0.80*	*0.83*	*0.78*	*0.66*	*0.89*	*0.80*	*0.41*	*0.43*
MLDi	mean	0.02	0.28	**0.38**	**0.57**	**0.33**	0.01	0.14	**0.38**	**-0.53**	**-0.29**
	min	*-0.14*	*-0.03*	*0.18*	*0.36*	*0.15*	*-0.36*	*-0.07*	*-0.12*	*-0.67*	*-0.46*
	max	*0.13*	*0.59*	*0.65*	*0.80*	*0.61*	*0.50*	*0.31*	*0.61*	*0.03*	*-0.14*
SSSi	mean	0.21	**0.31**	0.22	0.52	0.08	-0.24	0.33	0.39	-0.29	**-0.37**
	min	*-0.19*	*-0.05*	*0.02*	*0.33*	*-0.17*	*-0.49*	*0.04*	*0.03*	*-0.37*	*-0.71*
	max	*0.33*	*0.55*	*0.40*	*0.63*	*0.31*	*-0.12*	*0.45*	*0.54*	*0.03*	*0.04*

3.3 Regression analysis

A regression model has been set up for each of the regions and both timescales, based on the findings from the composite maps and the index correlation analysis. The predictors chosen for the regression models have been chosen to provide the best possible regression model, not only focusing on the linear relationship between the predictors and the CO_2 flux as shown in the index analysis (Table 3). Some predictors might show a weak correlation coefficient, but contribute to a higher degree of explanation in combination with other predictors. For instance the NAO index is not considered for the regression models, as it to some degree represents the same dynamics as the wind index, and therefore does not contribute to a higher degree of explanation for the regression models. In the following, the descriptions of the regression models is based on the mean R^2 value of the 10 ensemble members for each region (Table 4). The regression models for the interannual variability shows slightly higher correlation/explanation for the CO_2 flux variability in the different regions compared to the decadal variability. In general, the NA region shows the lowest degree of correlation on both timescales, emphasising the need to divide the region into smaller regions.

      The North Atlantic region interannual CO_2 flux can be explained by 0.48 R^2 by the variability in AMOC and wind speed (Table 4). The spatial patterns show a strong, homogeneous positive wind anomaly correlates well with a positive CO_2 flux anomaly in the NA (Fig. 3). Furthermore, the index analysis shows that both the AMOCi and Wi correlates well with the CO_2 flux variability (0.40 and 0.68, respectively, Table 3). The wind speed is expected to be driving the CO_2 flux variability, but the AMOCi represents a more dynamic control on the variability. The decadal timescale regression model includes predictors as SPGi, SSSi and Wi. Here, the R^2 value is 0.37 (Table 4). The composite map does not show a strong spatial pattern between the predictors and the CO_2 flux variability, which might explain the lower R^2 value. The predictors chosen for the decadal regression model align with the indexes with the greatest correlation as seen in Table 3.

      The Nordic Seas region shows a good degree of explanation (0.62 and 0.58 for the interannual and decadal timescales respectively, Table 4) based on MLDi, SICi and Wi. The sea ice concentration works as a main driver for the CO_2 flux variability in the NS as discussed earlier and seen in Fig. 4. Furthermore, a strong positive signal in the MLD anomaly correlates with the CO_2 flux anomaly, indicating that dynamical processes, such as strengthening of the NSG (a deepening of the SSH) and increased convection related to disappearing sea ice also controls the CO_2 flux variability in the NS. The index correlation analysis also indicates the wind stress as a controlling parameter in this region in both timescales (Table 4). The fact that the regression model is based on the same parameters for both timescales indicates that the processes driving the CO_2 flux variability is stable across timescales for this region.

      The Nordic Seas East region shows a high degree of explanation as well (0.68 and 0.53 interannual and decadal respectively, Table 4). The interannual predictors being MLDi, SSTi and Wi and the decadal NSGi, AMOCi and Wi. The interannual and decadal variability is well explained by the spatial patterns in the region (Fig. 5). However, the index analysis show a weak linear correlation between the predictors SSTi and AMOCi and the CO_2 flux on the interannual and decadal timescale respectively (Table 3). The low correlation coefficient in the index analysis does not however rule out, that

the SST and AMOC contribute to the variability combined with other predictors, as shown in the regression models for the region. The NSE regression models show that dynamical processes such as ocean mixing and circulation drive the CO_2 flux variability within the region in addition to physical parameters such as SST and wind, which is expected from the gas transfer equations (Eq. 1-3).

640   The western part of the Subpolar region shows the next best degree of correlation on the interannual timescale (0.68 interannual and 0.50 decadal, Table 4). The regression model setup based on the interannual variability entails AMOCi, SSTi, and Wi and show a R^2 value of 0.68. Based on MLDi, SSTi and Wi the regression model for the variability on decadal timescale show a R^2 value of 0.50. We expected dynamic ocean processes such as the SPG strength to be controlling the CO_2 flux in the region, however the regression model show that the AMOCi and MLDi are predictors representing the dynamic

645 ocean processes. The SST anomaly shows a negative anomaly on the interannual timescale and a positive anomaly on the decadal timescale, both correlating with a positive CO_2 flux anomaly (Fig. 6), which is also evident in the negative and postive correlation of the SSTi in the index analysis on interannual and decadal timescale, respectively (Table 3). This shows that the relationship between the predictors might not be linearly, and that they in combination contribute to the CO_2 flux variability even though they individually do not contribute.

650   Lastly, the CO_2 flux variability in the SPE region is controlled by SST and MLD on both timescales, however, the interannual regression model also includes Wi, and the decadal regression model includes SSSi, as indicated in Fig. 7. The R^2 values of the regression models show that the correlation is better on the interannual timescale (0.55) than the decadal timescale (0.40) (Table 4). Here, the regression model analysis shows that besides expected drivers such as SST and SSS (as discussed earlier and based on Eq.1-3), dynamical processes such as ocean mixing also drives the CO_2 flux variability. The

655 MLD variability points to the SPE being a dynamical region, maybe affected by the SPG circulation in the western part of the Subpolar region. Furthermore, SPE is an ice-free region, allowing us to understand the dynamics of the CO_2 flux variability without the strong SIC driver. The decadal regression model for the SPE is the only one not including the Wi. The wind speed anomaly is both negative and positive within the region, which indicates that the wind speed might not be a controlling factor in the SPE (Fig. 7).

Table 4
Applied regressions for all regions across timescales. R^2 values based on mean R^2 for all ten ensemble members in interannual (int) and decadal (dec) timescales

	NA		NS		NSE		SPW		SPE	
	Predictors	R^2	Predictors	R^2	Predictors	R^2	Predictors	R^2	Predictors	R^2
Int	AMOCi, Wi	0.48	MLDi, SICi, Wi	0.62	MLDi, SSTi, Wi	0.68	AMOCi, SSTi, Wi	0.68	SSTi, MLDi, Wi	0.55
Dec	SPGi, SSSi, Wi	0.37	MLDi, SICi, Wi	0.58	NSGi, AMOCi, Wi	0.53	MLDi, SSTi, Wi	0.50	SSSi, MLDi, SSTi	0.40

4. Discussion

4.1 Biases in ESMs

We calculated the CO_2 flux using the dependent parameters from the model as seen in Eq 1-3 to test to what degree the model CO_2 flux could be reproduced. Using monthly mean fields of SST, SSS, ΔpCO_2 and wind speed we are able to
665 reproduce the CO_2 flux variability, however to reproduce the total flux we need to use a scaled wind field (wind x 1.2). PISCES calculates the air-sea CO_2 flux daily (Döscher et al., 2021; Aumont et al., 2015), and by using monthly mean fields (as is the available data) we risk a smoothening of the actual daily variability that can explain the need for a scaled wind field. Turner et al. (1996) discusses how using monthly mean fields for wind and temperature can affect the calculation of atmosphere–ocean fluxes (in their study dimethyl sulphide fluxes in the Nordic Seas, however using Wanninkhof (1992) gas
670 transfer equations as in this study, Eq. 1-3). Reproducing the CO_2 flux helps us understand the sensitivity and dependencies on the physical parameters used to calculate the flux. The wind speed field shows a big sensitivity, which is also emphasised in the regression models, all but one entailing the Wi.

Earth System Models inevitably simplify the complex climate system, which will introduce biases to the modelled processes. One example being the monthly mean wind field that introduces a bias in the calculated CO_2 flux. Another bias
675 addressed in this paper is the SIC bias in EC-Earth3-CC. As stated by Döscher et al., 2022; Tian et al., 2021 and shown in Fig. 1b EC-Earth3 (and thereby EC-Earth3-CC) shows an overestimation of the SIC in the Nordic Seas and the North Atlantic. The index and regression model analysis of the NS shows that the SIC is a driver of the CO_2 flux variability, as expected based on Eq. 3. Therefore, the overestimation of sea ice extent and concentration in EC-Earth3 will undoubtebly affect and possibly control the CO_2 flux variability in the ocean in the EC-Earth3-CC runs. However, even in regions of sea-
680 ice such as the SPW and the NA, SIC does not exclude significant impact of other processes, as SIC is not regarded as a predictor for the CO_2 flux variability in these regions (Table 3, 4).

4.2 Predictors

Our analysis demonstrated that the CO_2 flux variability and its drivers cannot be assesed meaningsully considering the larger
685 northern North Atlantic region; but instead needs to be stratified at a regional and sub-basin level. Our analysis shows a high degree of explained variability of the CO_2 flux within the regions defined including dynamically separated ocean regions (Table 4). Based on the regression models we have established, that a linear correlation between the CO_2 flux and other predictors will not allow us to explain and understand the full CO_2 flux variability. It is clear that internal dynamics between the different predictors also affect the CO_2 flux variability as shown in section 3.3. Furthermore, we also establish that not
690 only the physical parameters SST, SSS and wind speed work as drivers of the CO_2 flux in the regions. It is evident that wind speed poses a great control on the CO_2 flux variability as discussed earlier, but we also see dynamic predictors such as ocean mixing (MLDi), gyre circulation (NSGi/SPGi) and larger scale ocean circulation and transport (AMOC) as drivers. Holliday

Deleted: '

Deleted: and

Deleted: s

Deleted: ies

Deleted: ed

Deleted: a

Deleted: considered across

Deleted: ,

Deleted: and demonstrate

Deleted: specifics

Deleted: However, o

Deleted: demonstrate that it is possible to

Deleted:

Deleted: variability

Deleted: smaller

Deleted: to a good degree

Deleted: t

et al. (2020) and Hátún et al. (2005, 2017) discuss how the larger scale dynamics such as the gyre circulation (SPG and NSG) and AMOC variability affect the SST, SSS and PP in the northern North Atlantic, aligning with our findings. Despite being the smallest region in terms of area among these studies (Table 2), the NSE region exhibits the highest variability and mean flux. This remains the case until 1960 (Fig. 2), when the SPW and NSE flux time series converge. Our regression analysis yields the highest R^2 values in the NSE and SPW regions (Table 4), underscoring the robustness of our approach. Notably, the fact that our regression models provide the strongest explanatory power in the regions with the greatest variability and mean CO_2 flux suggests a stable and reliable representation of the system dynamics.

Throughout our analysis we have established that a deepening of the MLD often coincides with a positive CO_2 flux anomaly, which in some cases can be explained by a deepening of the MLD resulting in an increase in DIC in the surface layer, decreasing pCO$_2$ in the surface layer and thus increasing the atmosphere-ocean CO_2 flux (Fig 3-6). However, we also see the deepening of the MLD as a response to a decrease in SIC, resulting in convection and an increase in the atmosphere–ocean CO_2 flux, which is especially evident in the NS region (Fig 4). The index analysis also shows a positive correlation between MLD and CO_2 flux in all the regions except for the SPE (Table 3). However, counter-intuitively to what is earlier established in our composite map analysis, we see a (strong) negative correlation between MLD and the CO_2 flux, both spatially and in the index analysis in the SPE region as mentioned (Fig. 7, Table 3). The MLDi is one of the predictors defining the regression models for both timescales in the SPE, which means that the MLD variability explains a big part of the CO_2 flux variability, despite their counter-intuitive negative correlation. The spatial patterns of the SPE shows a negative mirroring between the CO_2 flux and both SSS and SST most evident on the longer timescale, but also to some degree on the short timescale (Fig. 7). Furthermore, the spatial patterns also show a possible blocking of the North Atlantic current, indicated by a closed gyre system building up SSH. The blocking of the North Atlantic current might allow for fresh, cold and nutrient-rich Arctic water to enter the system, resulting in a positive CO_2 flux anomaly due to a decrease in temperature and nutrient supply increasing the PP and thus the CO_2 uptake. Increased freshwater supply from the Arctic would also result in increased stratification of the water column, indicated by the shallowing of the MLD and thereby the negative correlation between the CO_2 flux and MLD. We have also found that in EC-Earth3-CC, PP and SSS are more or less replaceable, including spatial patterns and their correlation. The North Atlantic is strongly influenced by the AMOC and SPG circulation, both regulating the salinity distribution and nutrient transport. The change in SSS reflects changes in the balance of freshwater input (i.e. freshwater from the Arctic). Both SSS and PP are sensitive to these large scale circulation dynamics, and they might co-vary, making them somewhat interchangeable in ESMs. These observations indicate that CO_2 flux variability in the northern North Atlantic cannot be adequately explained by individual predictors in a linear framework. Instead, a comprehensive understanding of the underlying processes and the interactions among predictors is essential to accurately capture atmosphere-ocean CO_2 flux variability.

Deleted: ,

Deleted: r

Deleted: i

Deleted: correlates

Deleted: with

Deleted: We see this correlation both in the spatial patterns and in t

Deleted: (Fig. 3-6,

Deleted: C

Deleted: Additionally, t

Deleted: correlation

Deleted: on both timescales

Deleted: o

Deleted: is

Deleted: '

Deleted: -

4.3 Future projections

Based on the results of our regression model analysis we expect that the regression models are robust also for assessing the CO_2 flux variability and tendencies in the North Atlantic from scenario simulations without a carbon cycle (EC-Earth3). This would be beneficial for estimating uncertainties related to future CO_2 uptake and in general to understand the carbon cycle impacts of regional climate change patterns. We have purposely defined the regression models by using non-biogeochemical predictors only. Studies have looked into the predictability of interannual-to-decadal variability: Li et al., 2016 show a predictive skill of CO_2 uptake in the western SPG of up to 4-7 years based on a ESM prediction system. They conclude, that the predictive skill is attributed to the combination of improved ocean physical states and circulation variability, primarily in winter which corroborates our approach. Ilyina et al., 2020 shows a predictive skill for the global ocean carbon sink of up to 6 years for some EMSs. Further motivation for focussing on dynamical indices comes from Fransner et al., 2020. They show that the predictability of ocean carbon uptake correlates well with the predictability of the MLD, suggesting that the predictable signal comes from exchange of DIC with deep waters.

Looking into the near future, studies consistently establish that the warming of the global climate system is also manifested in warming of the ocean (Fox-Kemper et al., 2021; Bopp et al., 2013; Fu et al., 2016; Laufkötter et al., 2016; Liu et al., 2023 Kwiatowski et al., 2020). Ocean temperature increase would from first principles result in a decreased atmosphere–ocean CO_2 flux through the effects on solubility, however, as demonstrated in this study the CO_2 flux variability is more complex than simple linear relationships with temperature. For example, an increased ocean temperature will lead to a melting of the sea ice in the northern North Atlantic, resulting in more open ocean surface that can take up CO_2. However, a warming ocean will also affect the ocean circulation, both the large scale circulation and the small scale ocean mixing. AMOC is predicted to slow down with global warming (McKinley et al., 2023; Liu et al., 2023). Stagnating ocean circulation in the North Atlantic will as seen in our analysis affect the CO_2 flux variability in particular the SPW region of the NA, but also further north in the NSE region. Furthermore, a warming ocean combined with melting ice and stagnated ocean circulation could result in increased upper ocean stratification, reduced MLD and less exchange with high DIC water masses in the deeper ocean. The predicted global warming will possibly result in stronger winds in the North Atlantic region (Lee et al., 2021, Ruosteenoja et al., 2019) which based on the gas exchange equation and our results will contribute to increasing the atmosphere–ocean CO_2 flux. Our results identify SIC and wind speed as main drivers of the CO_2 flux variability in a number of subregions of the northern North Atlantic, which would indicate an increase in ocean CO_2 uptake in the near future but counteracted by the direct temperature effect.

To expand the regression analysis to investigate their robustness in scenario runs using other ESM's it is pivotal to have an in-depth understanding of the model setup and of the characteristics of indices in the specific model including biases and variability. Examples that might complicate the applicability of the regression models from this study could be how the gas transfer is handled across sea ice, how realistic the separate indices are compared to observations and how the indices

840 relate to each other. Our analysis provides a framework for identifying the key predictors and processes driving atmosphere-ocean CO_2 flux variability in the northern North Atlantic, but further work is necessary before applying the framework across other ESM's. We demonstrate that physical ocean and atmospheric parameters alone account for a significant portion of this variability, offering a valuable approach for assessing and understanding future CO_2 flux changes using readily available climate model and ocean reanalysis data.

845 **5. Conclusion**

Our analysis highlights the critical role of physical and dynamical processes in shaping CO_2 flux variability across the northern North Atlantic. Using historical simulations from the EC-Earth3-CC model, we show that key drivers, including SIC, SST, SSS, and wind stress, and ocean dynamics such as mixing and circulation, exert regionally and temporally varying influences on the atmosphere–ocean CO_2 fluxes. While our regression models achieve high explanatory power, they capture

850 interannual variability more effectively than decadal trends, underscoring the dominant role of short-term fluctuations. Furthermore, our findings reveal that CO_2 flux variability cannot be attributed to simple linear relationships with individual predictors but instead emerges from complex interactions among multiple processes. Notably, wind stress exerts a particularly strong influence, aligning with expectations from gas transfer formulations. These results emphasize the spatially and temporally dependent nature of ocean carbon uptake and highlight the need for a multifaceted approach when assessing

855 future CO_2 flux variability in a changing climate. Additionally, we conclude that the regression models we have defined in our analysis can serve as a framework for predicting and understanding future atmosphere–ocean CO_2 fluxes in the ESM realm. The main conclusion is that the CO_2 flux variability cannot be attributed to simple linear relationships with individual predictors, but instead emerges from complex interactions among multiple processes.

860

Author contributions. SMO and AP conceived and designed the study. AP wrote the majority of the manuscript, while SMO provided supervision and guidance in analysing and interpreting the results. SMO and CRL contributed to the writing and revision of the manuscript.

865 *Code/data availability*. EC-Earth3-CC data is available through ESGF (*https://aims2.llnl.gov/search/cmip6/*) and postprocessing scripts are available upon request.

Competing interest. The authors declare that they have no known competing financial interests or personal relationships that could have appeared to influence the work reported in this paper. One of the authors, CRL, serves as an Associate Editor for

870 Biogeosciences.

¶

875 *Financial support*. AP was supported by SDU's climate cluster, EU Horizon Ocean observations and indicators for climate and assessments, ObsSea4Clim, Grant agreement ID: 101136548, 10.3030/101136548 Internal contribution Nr. 15, NCKF/DMI, the Villum Foundation (grant no. 29411) and by Danmarks Fri Forskningsfond (DFF, Carolin R. Löscher, grant no. 4283-00265B).

References

Ardyna, M. and Arrigo, K.R.: Phytoplankton dynamics in a changing Arctic Ocean. *Nature Climate Change*, *10*(10), pp.892-903, https://doi.org/10.1038/s41558-020-0905-y, 2020.

Aumont, O., Éthé, C., Tagliabue, A., Bopp, L. and Gehlen, M.: PISCES-v2: an ocean biogeochemical model for carbon and ecosystem studies. Geoscientific Model Development Discussions, 8(2), pp.1375-1509, https://doi.org/10.5194/gmd-8-2465-885   2015, 2015

Berx, B. and Payne, M.R.: The Sub-Polar Gyre Index–a community data set for application in fisheries and environment research. Earth System Science Data, 9(1), pp.259-266, https://doi.org/10.5194/essd-9-259-2017, 2017

Bopp, L., Resplandy, L., Orr, J. C., Doney, S. C., Dunne, J. P., Gehlen, M., Halloran, P., Heinze, C., Ilyina, T., Séférian, R., Tjiputra, J., Vichi, M.: Multiple stressors of ocean ecosystems in the 21st century: projections with CMIP5 models. 890   Biogeosciences. 10, 6225-6245, doi: 10.5194/bg-10-6225-2013, 2013

Boyd, P.W. and Trull, T.W.: Understanding the export of biogenic particles in oceanic waters: Is there consensus? Progress in Oceanography, 72(4), 276-312, https://doi.org/10.1016/j.pocean.2006.10.007, 2007

Breeden, M. L. and McKinley, G. A.: Climate impacts on multidecadal pCO 2 variability in the North Atlantic: 1948–2009, Biogeosciences, 13, 3387-3396, https://doi.org/10.5194/bg-13-3387-2016, 2016.

895   Broecker, W.S., Takahashi, T., Simpson, H.J. and Peng, T.H.: Fate of fossil fuel carbon dioxide and the global carbon budget. Science, 206(4417), pp.409-418, https://doi.org/10.1126/science.206.4417.409, 1979

Esbensen, S.K. and Reynolds, R.W.: Estimating monthly averaged air-sea transfers of heat and momentum using the bulk aerodynamic method. Journal of physical oceanography, 11(4), pp.457-465, https://doi.org/10.1175/1520-0485(1981)011%3C0457:EMAAST%3E2.0.CO;2, 1981

900   Daniault, N., Mercier, H., Lherminier, P., Sarafanov, A., Falina, A., Zunino, P., Pérez, F.F., Ríos, A.F., Ferron, B., Huck, T. and Thierry, V.: The northern North Atlantic Ocean mean circulation in the early 21st century. Progress in Oceanography, 146, pp.142-158, https://doi.org/10.1016/j.pocean.2016.06.007, 2016

Döscher, R., Acosta, M., Alessandri, A., Anthoni, P., Arneth, A., Arsouze, T., Bergmann, T., Bernadello, R., Bousetta, S., Caron, L.P. and Carver, G.: The EC-earth3 Earth system model for the climate model intercomparison project 905   6. Geoscientific Model Development Discussions, 2021, pp.1-90, https://doi.org/10.5194/gmd-15-2973-2022, 2021

Friedlingstein, P., O'Sullivan, M., Jones, M.W., Andrew, R.M., Hauck, J., Landschützer, P., Le Quéré, C., Li, H., Luijkx, I.T., Olsen, A. and Peters, G.P.: Global carbon budget 2024. Earth System Science Data Discussions, 2024, pp.1-133, https://doi.org/10.5194/essd-2024-519, 2024

915 Foukal, N.P. and Lozier, M.S.: Assessing variability in the size and strength of the N orth A tlantic subpolar gyre. Journal of Geophysical Research: Oceans, 122(8), pp.6295-6308, https://doi.org/10.1002/2017JC012798, 2017

Fox-Kemper, B., Hewitt, H.T., Xiao, C., Aðalgeirsdóttir, G., Drijfhout, S.S., Edwards, T.L., Golledge, N.R., Hemer, M., Kopp, R.E., Krinner, G., Mix, A., Notz, D., Nowicki, S., Nurhati, I.S., Ruiz, L., Sallée, J.-B., Slangen, A.B.A, Yu, Y.: Ocean, Cryosphere and Sea Level Change. In Climate Change 2021: The Physical Science Basis. Contribution of Working

920 Group I to the Sixth Assessment Report of the Intergovernmental Panel on Climate Change [Masson-Delmotte, V., P. Zhai, A. Pirani, S.L. Connors, C. Péan, S. Berger, N. Caud, Y. Chen, L. Goldfarb, M.I. Gomis, M. Huang, K. Leitzell, E. Lonnoy, J.B.R. Matthews, T.K. Maycock, T. Waterfield, O. Yelekçi, R. Yu, and B. Zhou (eds.)]. Cambridge University Press, Cambridge, United Kingdom and New York, NY, USA, pp. 1211–1362, doi:10.1017/9781009157896.011, 2021

Fransner, F., Counillon, F., Bethke, I., Tjiputra, J., Samuelsen, A., Nummelin, A. and Olsen, A.: Ocean biogeochemical
925 predictions—initialization and limits of predictability. Frontiers in Marine Science, 7, p.386, https://doi.org/10.3389/fmars.2020.00386, 2020.

Fu, W., Randerson, J. T., Moore, J. K.: Climate change impacts on net primary production (NPP) and export production (EP) regulated by increasing stratification and phytoplankton community structure in CMIP5 models. Biogeosciences, 13, 5151-5170, doi: 10.5194/bg-13-5151-2016, 2016.

930 Gruber N., Keeling, C. D., Bates, N. R.: Interannual variability in the North Atlantic Ocean carbon sink. Science, 298, 2374-2378, doi:10.1126/science.1077077, 2002.

Gregor, L. & Fay, A.: SeaFlux: harmonised sea-air CO2 fluxes from surface pCO2 data products using a standardised approach (2021.04.03) [Data set]. Zenodo, https://doi.org/10.5281/zenodo.5482547, 2021.

Gruber, N., Clement, D., Carter, B.R., Feely, R.A., Van Heuven, S., Hoppema, M., Ishii, M., Key, R.M., Kozyr, A., Lauvset,
935 S.K. and Lo Monaco, C.: The oceanic sink for anthropogenic CO2 from 1994 to 2007. Science, 363(6432), pp.1193-1199, https://doi.org/10.1126/science.aau5153, 2019

Gruber, N., Bakker, D.C., DeVries, T., Gregor, L., Hauck, J., Landschützer, P., McKinley, G.A. and Müller, J.D.: Trends and variability in the ocean carbon sink. Nature Reviews Earth & Environment, 4(2), pp.119-134, https://doi.org/10.1038/s43017-022-00381-x, 2023

940 Hátún, H., Sandø, A.B., Drange, H., Hansen, B. and Valdimarsson, H.: Influence of the Atlantic subpolar gyre on the thermohaline circulation. Science, 309(5742), pp.1841-1844, https://doi.org/10.1126/science.1114777, 2005

Hátún, H., Azetsu-Scott, K., Somavilla, R., Rey, F., Johnson, C., Mathis, M., Mikolajewicz, U., Coupel, P., Tremblay, J.É., Hartman, S. and Pacariz, S.V.: The subpolar gyre regulates silicate concentrations in the North Atlantic. Scientific reports, 7(1), p.14576, https://doi.org/10.1038/s41598-017-14837-4, 2017

945 Häkkinen, S., Rhines, P.B. and Worthen, D.L.:. Northern North Atlantic sea surface height and ocean heat content variability. Journal of Geophysical Research: Oceans, 118(7), pp.3670-3678, https://doi.org/10.1002/jgrc.20268, 2013

Holliday, N.P., Bersch, M., Berx, B., Chafik, L., Cunningham, S., Florindo-López, C., Hátún, H., Johns, W., Josey, S.A., Larsen, K.M.H. and Mulet, S.: Ocean circulation causes the largest freshening event for 120 years in eastern subpolar North Atlantic. Nature communications, 11(1), p.585, https://doi.org/10.1038/s41467-020-14474-y, 2020

950 Hughes, P.J., Bourassa, M.A., Rolph, J.J. and Smith, S.R.: Averaging-related biases in monthly latent heat fluxes. Journal of Atmospheric and Oceanic Technology, 29(7), pp.974-986, https://doi.org/10.1175/JTECH-D-11-00184.1, 2012

Ilyina, T., Li, H., Spring, A., Müller, W.A., Bopp, L., Chikamoto, M.O., Danabasoglu, G., Dobrynin, M., Dunne, J., Fransner, F. and Friedlingstein, P.: Predictable variations of the carbon sinks and atmospheric CO2 growth in a multi-model framework. Geophysical Research Letters, 48(6), https://doi.org/10.1029/2020GL090695, 2021.

955 Jones, C.D., Arora, V., Friedlingstein, P., Bopp, L., Brovkin, V., Dunne, J., Graven, H., Hoffman, F., Ilyina, T., John, J.G. and Jung, M.: C4MIP–The coupled climate–carbon cycle model intercomparison project: Experimental protocol for CMIP6. Geoscientific Model Development, 9(8), pp.2853-2880, https://doi.org/10.5194/gmd-9-2853-2016, 2016

Kerr, R.A.: A North Atlantic climate pacemaker for the centuries. Science, 288(5473), pp.1984-1985, https://doi.org/10.1126/science.288.5473.1984, 2000

960 Khatiwala, S., Primeau, F., and Hall, T.: Reconstruction of the history of anthropogenic CO2 concentrations in the ocean, Nature, 462, 346-349, https://doi.org/10.1038/nature08526, 2009

Khatiwala, S., Tanhua, T., Mikaloff Fletcher, S., Gerber, M., Doney, S.C., Graven, H.D., Gruber, N., McKinley, G.A., Murata, A., Ríos, A.F. and Sabine, C.L.: Global ocean storage of anthropogenic carbon, Biogeosciences, 10(4), pp.2169-219, https://doi.org/10.5194/bg-10-2169-2013, 2013

965 Kwiatkowski, L., Torres, O., Bopp, L., Aumont, O., Chamberlain, M., Christian, J. R., Dunne, J. P., Gehlen, M., Ilyina, T., John, J. G., Lenton, A., Li, H., Lovenduski, N. S., Orr, J. C., Palmieri, J., Santana-Falcón, Y., Schwinger, J., Séférian, R., Stock, C. A., Tagliabue, A., Takano, Y., Tjiputra, J., Toyama, K., Tsujino, H., Watanabe, M., Yamamoto, A., Yool, A., and Ziehn, T.: Twenty-first century ocean warming, acidification, deoxygenation, and upper-ocean nutrient and primary production decline from CMIP6 model projections, Biogeosciences, 17, 3439–3470, https://doi.org/10.5194/bg-17-3439-

970 2020, 2020.

Landschützer, P., Gruber, N. and Bakker, D.C.: Decadal variations and trends of the global ocean carbon sink. Global Biogeochemical Cycles, 30(10), pp.1396-1417, https://doi.org/10.1002/2015GB005359, 2016

Laufkötter, C., Vogt, M., Gruber, N., Aumont, O., Bopp, L., Doney, S. C., Dunne, J. P., Hauck, J., John, J. G., Lima, I. D., Seferian, R., Völker, C.: Projected decreases in future marine export production: the role of the carbon flux through the

975 upper ocean ecosystem. Biogeosciences, 13, 4023-4047, doi:10.5194/bg-13-4023-2016, 2016

Le Quéré, C., Moriarty, R., Andrew, R.M., Canadell, J.G., Sitch, S., Korsbakken, J.I., Friedlingstein, P., Peters, G.P., Andres, R.J., Boden, T.A. and Houghton, R.A.: Global carbon budget 2015. Earth System Science Data, 7(2), pp.349-396, https://doi.org/10.5194/essd-7-349-2015, 2015

Le Quéré, C., Andrew, R.M., Friedlingstein, P., Sitch, S., Hauck, J., Pongratz, J., Pickers, P.A., Korsbakken, J.I., Peters,

980   G.P., Canadell, J.G. and Arneth, A.: Global carbon budget 2018. Earth System Science Data, 10(4), pp.2141-2194, https://doi.org/10.5194/essd-10-2141-2018, 2018

Lee, J.-Y., Marotzke, J., Bala, G., Cao, L., Corti, S., Dunne, J.P., Engelbrecht, F., Fischer, E., Fyfe, J.C., Jones, C., Maycock, A., Mutemi, J., Ndiaye, O., Panickal, S., Zhou, T.:Future Global Climate: Scenario-Based Projections and Near-Term Information. In Climate Change 2021: The Physical Science Basis. Contribution of Working Group I to the Sixth

985   Assessment Report of the Intergovernmental Panel on Climate Change [Masson-Delmotte, V., P. Zhai, A. Pirani, S.L. Connors, C. Péan, S. Berger, N. Caud, Y. Chen, L. Goldfarb, M.I. Gomis, M. Huang, K. Leitzell, E. Lonnoy, J.B.R. Matthews, T.K. Maycock, T. Waterfield, O. Yelekçi, R. Yu, and B. Zhou (eds.)]. Cambridge University Press, Cambridge, United Kingdom and New York, NY, USA, pp. 553–672, doi:10.1017/9781009157896.006, 2021.

Leseurre, C., Lo Monaco, C., Reverdin, G., Metzl, N., Fin, J., Olafsdottir, S. and Racapé, V.: Ocean carbonate system

990   variability in the North Atlantic Subpolar surface water (1993–2017). Biogeosciences, 17(9), pp.2553-2577, https://doi.org/10.5194/bg-17-2553-2020, 2020

Li, H., Ilyina, T., Müller, W.A. and Sienz, F.: Decadal predictions of the North Atlantic CO2 uptake. Nature communications, 7(1), p.11076, https://doi.org/10.1038/ncomms11076, 2016

Liu, Y., Moore, J.K., Primeau, F. et al. Reduced CO_2 uptake and growing nutrient sequestration from slowing overturning

995   circulation. Nat. Clim. Chang. 13, 83–90, https://doi.org/10.1038/s41558-022-01555-7, 2023

McKinley. G. A., Bennington, V., Meinshausen, M., Nicholls, Z.: Modern air-sea flux distributions reduce uncertainty in the future ocean carbon sink. Environ. Res. Lett. 18, 044011, doi:10.1088/1748-9326/acc195, 2023.

Madec, G.: NEMO ocean engine, 2015.

Mikaloff Fletcher, S. E., Gruber, N., Jacobson, A. R., Doney, S. C., Dutkiewicz, S., Gerber, M., Follows, M., Joos, F.,

1000   Lindsay, K., Menemenlis, D., Mouchet, A., Müller, S. A., and Sarmiento, J. L.: Inverse estimates of anthropogenic CO2 uptake, transport, and storage by the ocean, Global Biogeochemical Cycles, 20, https://doi.org/10.1029/2005GB002530, 2006.

Orvik, K.A.: Long-term moored current and temperature measurements of the Atlantic inflow into the Nordic Seas in the Norwegian Atlantic Current; 1995–2020. Geophysical Research Letters, 49(3), doi: https://doi.org/10.1029/2021GL096427,

1005   2022

Polyakov, I.V., Beszczynska, A., Carmack, E.C., Dmitrenko, I.A., Fahrbach, E., Frolov, I.E., Gerdes, R., Hansen, E., Holfort, J., Ivanov, V.V. and Johnson, M.A.: One more step toward a warmer Arctic. Geophysical Research Letters, 32(17), https://doi.org/10.1029/2005GL023740, 2005

Ruosteenoja, K., Vihma, T. and Venäläinen, A.: Projected changes in European and North Atlantic seasonal wind climate

1010   derived from CMIP5 simulations. Journal of Climate, 32(19), pp.6467-6490, https://doi.org/10.1175/JCLI-D-19-0023.1, 2019.

Sabine, C. L., Feely, R. A., Gruber, N., Key, R. M., Lee, K., Bullister, J. L., Wanninkhof, R., Wong, C., Wallace, D. W., and Tilbrook, B.: The oceanic sink for anthropogenic CO2, science, 305, 367-371, https://doi.org/10.1126/science.1097403, 2004.

1015 Sanders, R., Henson, S.A., Koski, M., Christina, L.D.L.R., Painter, S.C., Poulton, A.J., Riley, J., Salihoglu, B., Visser, A., Yool, A., Bellerby, R.: The biological carbon pump in the North Atlantic. Progress in Oceanography, 129, 200-218, https://doi.org/10.1016/j.pocean.2014.05.005, 2014.

Schulzweida, U., Müller, R., Kornblüh, L., Ansorge, C. and Quast, R.: CDO–Climate Data Operators–v2. 5.0. Center for Marine and Atmospheric Sciences (ZMAW), Max-Planck Institute for Meteorology, University of Hamburg,

1020 https://code.mpimet.mpg.de/projects/cdo/embedded/index.html (last update: November 2024), 2012

Sigman, D. M. and Boyle, E.A.: Glacial/interglacial variations in atmospheric carbon dioxide. Nature, 407(6806), 859-869, https://doi.org/10.1038/35038000, 2000.

Simmonds, I. and Dix, M.: The use of mean atmospheric parameters in the calculation of modeled mean surface heat fluxes over the world's oceans. Journal of physical oceanography, 19(2), pp.205-215, https://doi.org/10.1175/1520-

1025 0485(1989)019%3C0205:TUOMAP%3E2.0.CO;2, 1989

Takahashi, T., Broecker, W.S. and Langer, S.: Redfield ratio based on chemical data from isopycnal surfaces. Journal of Geophysical Research: Oceans, 90(C4), pp.6907-6924, https://doi.org/10.1029/JC090iC04p06907, 1985.

Takashi, T., Sutherland, S. C., Wanninkhof, R., Sweeney, C., Feely, R. A., Chipman, D. W., Hales, B. Friederich, G., Chavez, F., and Sabine, C.: Climatological mean and decadal change in surface ocean pCO2, and net sea–air CO_2 flux over

1030 the global oceans. Deep Sea Research Part II: Topical Studies in Oceanography, 56, 554-577, https://doi.org/10.1016/j.dsr2.2008.12.009, 2009.

Terhaar, J., Frölicher, T.L. and Joos, F.: Observation-constrained estimates of the global ocean carbon sink from Earth system models. Biogeosciences, 19(18), pp.4431-4457, https://doi.org/10.5194/bg-19-4431-2022, 2022

Terhaar, J.: Drivers of decadal trends in the ocean carbon sink in the past, present, and future in Earth system

1035 models. Biogeosciences, 21(17), pp.3903-3926, https://doi.org/10.5194/bg-21-3903-2024, 2024

Thomas, M.D. and Zhang, R.: Two sources of deep decadal variability in the central Labrador Sea open-ocean convection region. Geophysical Research Letters, 49(11), p.e2022GL098825, https://doi.org/10.1029/2022GL098825, 2022

Tian, T., Yang, S., Karami, M.P., Massonnet, F., Kruschke, T. and Koenigk, T.: Benefits of sea ice initialization for the interannual-to-decadal climate prediction skill in the Arctic in EC-Earth3. Geoscientific Model Development, 14(7),

1040 pp.4283-4305, https://doi.org/10.5194/gmd-14-4283-2021, 2021

Turner, S.M., Malin, G., Nightingale, P.D. and Liss, P.S.: Seasonal variation of dimethyl sulphide in the North Sea and an assessment of fluxes to the atmosphere. Marine Chemistry, 54(3-4), pp.245-262, https://doi.org/10.1016/0304-4203(96)00028-X, 1996

Vancoppenolle M., Bopp, L., Madec, G., Dunne, J., Ilyina, T., Halloran, P. R., Steiner, N.: Future Arctic Ocean primary

1045 productivity from CMIP5 simulations: Uncertain outcome, but consistent mechanisms. Global Biogeochemical cycles, 27, 605-619, doi:10.1002/gbc.20055, 2013

Volkov, D.L., Smith, R.H., Garcia, R.F., Smeed, D.A., Moat, B.I., Johns, W.E. and Baringer, M.O.: Florida Current transport observations reveal four decades of steady state. Nature Communications, 15(1), p.7780, https://doi.org/10.1038/s41467-024-51879-5, 2024

1050 Wanninkhof, R.: Relationship between wind speed and gas exchange over the ocean. Journal of Geophysical Research: Oceans, 97(C5), pp.7373-7382, https://doi.org/10.1029/92JC00188, 1992

Wanninkhof, R.: Relationship between wind speed and gas exchange over the ocean revisited. Limnology and Oceanography: Methods, 12(6), pp.351-362, https://doi.org/10.4319/lom.2014.12.351, 2014

Zou, S., Bower, A.S., Lozier, M.S. and Furey, H.H.: Deep ocean circulation in the subpolar North Atlantic observed by

1055 acoustically-tracked floats. Progress in Oceanography, 211, p.102975, https://doi.org/10.1016/j.pocean.2023.102975, 2023

Yu, J., Menviel, L., Jin, Z.D., Thornalley, D.J.R., Foster, G.L., Rohling, E.J., McCave, I.N., McManus, J.F., Dai, Y., Ren, H. and He, F.: More efficient North Atlantic carbon pump during the last glacial maximum. Nature Communications, 10(1), p.2170, https://doi.org/10.1038/s41467-019-10028-z, 2019.

Page 9: [1] Deleted	Anna Pedersen	14/05/2025 14:27:00
Page 28: [2] Deleted	Anna Pedersen	06/05/2025 14:56:00
Page 28: [3] Deleted	Anna Pedersen	23/06/2025 11:29:00
Page 28: [4] Formatted	Anna Pedersen	14/05/2025 14:51:00

Indent: First line: 1,27 cm

Page 28: [5] Deleted	Anna Pedersen	23/06/2025 11:33:00
Page 28: [6] Deleted	Anna Pedersen	23/06/2025 11:39:00
Page 30: [7] Deleted	Anna Pedersen	14/05/2025 15:15:00